A constructive approach to assess the stability of anaerobic digestion systems

Mihaela Sbarciog[a,b], Alain Vande Wouwer[a]

[a]*Automatic Control Laboratory, University of Mons, Boulevard Dolez 31, B-7000 Mons, Belgium*
[b]*BioTeC+, KU Leuven, Gebroeders de Smetstraat 1, 9000 Ghent, Belgium*

Abstract

In this study, the steady states of an anaerobic digestion model are analytically computed and characterized. The influence of the dilution rate on the system states and methane outflow rate is illustrated by means of one-parameter bifurcation diagrams. A two-parameter bifurcation diagram is also computed. This diagram illustrates the combined effect of the dilution rate and inlet substrate concentration on the system steady states and allows to determine corrective actions (in terms of selecting appropriated inputs) for preserving system stability and efficiency. Expressions for all the boundaries and critical points appearing in the diagram are provided. Furthermore, the complex system behavior is illustrated by means of phase portraits. The paper emphasizes the methodology, which can also be applied to other bioprocesses taking place in continuously stirred tank reactors. The method allows practitioners to build two-parameter bifurcation diagrams by solving a set of algebraic equations. This implies low computational requirements.

Keywords: anaerobic digestion, bioreactor, nonlinear dynamics, bifurcation analysis]

1. Introduction

Anaerobic digestion allows the treatment of biodegradable wastewater and solid waste, i.e. the reduction of waste volume, and the production of biogas which can be exploited to generate electricity. Anaerobic digestion is achieved by several consortia of bacteria, and in a simplified view, 4 main steps can be distinguished: (a) hydrolysis of insoluble organic polymers, (b) acidogenesis which converts the soluble organic matter into volatile fatty acids and produces hydrogen, (c) acetogenesis where volatile fatty acids are converted to acetic acid, together with the

production of additional hydrogen (d) methanogenesis which finally leads to the production of biogas, a mixture of methane and carbon dioxide.

Anaerobic digestion is a technology of increasing importance, and it is now in widespread use in the sector of food and beverage, for the treatment of the effluents. However, anaerobic digestion processes can be delicate to operate due to their very slow transient phases and multiplicity of equilibrium points, influenced by the operating conditions, and uncontrolled fluctuations or perturbations in the inlet composition of the waste. Conservative operation policies [1, 2] are usually applied in order to avoid the risk of bioreactor wash-out and its dramatic consequences in terms of production loss. Hence, a detailed view on how the manipulated (dilution rate) and disturbance (substrate inlet concentration) inputs affect the process operation, provided by bifurcation analysis techniques, is certainly helpful in keeping the process stable and operating efficiently. Moreover, it provides also means for developing simple and efficient control strategies, which can be implemented on real anaerobic digestion systems with the available technology [3, 4].

Anaerobic digestion is modelled with different degrees of complexity and detail. A wide variety of models are available, ranging from the general anaerobic digestion model no.1 (ADM1) [5], which models all the stages appearing in the process and consists of 35 differential equations coupled with 8 algebraic equations, to simple models which describe only the methanogenesis step. The bifurcation analysis of anaerobic digestion models has been considered by many researchers, as the system complexity is reflected by its steady state multiplicity. The steady state analysis allows to detect the conditions which trigger the anaerobic digestion instability (or destabilization), that is generally assessed as the accumulation of volatile fatty acids and the lost ability of the system to produce biogas. To our knowledge, [6] is the only published study regarding the steady state behavior of the complex ADM1 model, where the authors used continuation software and investigated the influence of the dilution rate and inlet substrate concentration on the number and stability of the steady states. They concluded that up to ten coexisting steady states may occur under the same operating conditions.

By far, two-step models are the most used ones to describe the anaerobic digestion process. Shen et al. [7] presented the bifurcation and stability analysis of an anaerobic digestion model and concluded that the dynamics of such systems depend heavily on the Haldane-type kinetics describing the growth rate of methanogenic bacteria. Hess and Bernard [8] introduced a risk index for the operation of an anaerobic digestion system, which indicates whether the process has been triggered to a dangerous working mode. This index was defined based on

the areas of the stability regions of the system, which have been determined from the global analysis of the nonlinear dynamics. Sbarciog et al. [9] presented the analytical computation of the steady states and the bifurcation analysis of a two-step model. The analysis was performed taking into account the kinetics characteristics and not their explicit expressions. Subsequently, Sbarciog et al. [10] employed the bifurcation analysis and developed and implemented an algorithm to numerically estimate and visualize the stability boundary of the nominal equilibrium point of the anaerobic digestion model. Benyahia et al. [11] studied the equilibria and their stability considering qualitative properties of the kinetics for an anaerobic fixed-bed wastewater treatment process and proposed an overloading tolerance parameter to monitor the process on-line. Rincón et al. [12] presented a dynamic analysis for an anaerobic digester, based on the analytical application of the indirect Lyapunov method. The authors analytically compute the equilibria, the branches and the bifurcation points for a two-step model with Monod and Haldane kinetics for the acidogenesis and methanogenesis reactions.

Recently, Fekih-Salem et al. [13] studied an anaerobic digestion model with two reactions, ie. acidogenesis and hydrogenotrophic methanogenesis, and distinct removal rates. They established the necessary and sufficient conditions for the existence and local stability of all steady states for a general class of growth rates and constructed the operating diagrams which show the effect of the inhibition and the input substrate concentration (hydrogen) on the reduction of the coexistence region and the emergence of a bistability region. Khedim et al. [14] performed the mathematical analysis of an anaerobic digestion model for the treatment of protein-rich substrates and studied the influence of the control parameters on the process behavior. Operating diagrams were developed to illustrate the ideal conditions which optimize biogas yield and ammonia toxicity. Alzate-Ibanez et al. [15] employed the continuation package MatCONT ([16]) to numerically determine the operating diagrams of a two-step anaerobic digestion model that includes the influence of temperature and pH on the process kinetics. The bifurcation analysis led to the definition of safe and optimal operation regions for the bioreactor and the statement of two conditions for guaranteed optimum performance. These conditions were subsequently employed to propose a risk index that allowed the identification of possible destabilization in the bioreactor operation.

Although not of the same complexity as the ADM1 model in terms of number of states and biotransformations, the three-step models considered by Weedermann et al. [17, 18] show a similar complex steady state behavior. Weedermann et al. [17] studied in a first stage a three-step model without inhibition and assessed the system global stability using differential inequalities and conservation laws.

Subsequently, they derived conditions for existence, local stability, and bistability of equilibria and presented a global stability result also for the model with inhibition. Including biomass decay in the system dynamics, Weedermann et al. [18] showed that the model predicts increased biogas production in regions where the operating parameters, i.e. dilution rate and substrate inlet concentration push the system into a bistable state.

This paper presents the steady state analysis of the three-step mathematical model investigated by Weedermann et al. [18], without biomass decay, which has been considered negligible. In this paper a more engineering approach is employed to establish the results, which balances the mathematical developments with physical interpretations. The goal is to emphasize a methodology to perform the bifurcation analysis for different bioprocesses operated in continuous mode, which could be appealing to practitioners. This implies no use of specialized software, but algebraic equations which can be solved fastly and easily with the available computational technology. From this perspective, the anaerobic digestion model illustrates the type of complexity the methodology can manage to provide analytical results.

In this paper, analytical expressions of all system equilibria are provided and conditions for their occurrence are included. Since most of the steady states of the anaerobic digestion process are conditional equilibrium points, depending not only on the dilution rate but also on the inlet substrate concentration, a two-parameters bifurcation diagram is included. This diagram illustrates the regions in the input space (inlet concentration versus dilution rate) characterized by a different number of steady states. Such a bifurcation diagram may be obtained by using specialized, continuation software. However, the use of such software requires knowledge of systems dynamics and may not be obvious for practitioners. Therefore, this paper emphasizes a procedure that allows the analytical computation of the bifurcation diagram, by providing expressions for all the boundaries and critical points appearing on the diagram. These expressions are kinetics dependant, meaning that the kinetics structure is explicitly used in the calculations. However, the procedure is general and may be applied also to other bioprocesses. As a result, the bifurcation diagram is constructed by solving a collection of algebraic equations. In reference to the earlier work of the first author [9], the method described in this article is both a generalization and an extension. It represents a generalization as the class of systems (models defined in the methodology statement) is not restrictive and allows for the presence of all nutrients in the influent, leading naturally to the generalization of the results obtained for the two-step model used in the previous study. It represents an extension as it can accommodate models

where not all the nutrients are supplied with the inflow, the extreme case being illustrated in this study (extreme in the sense that only one substrate is supplied).

To keep a balance between mathematical derivations and practical interpretations, a detailed stability analysis of the equilibrium points in all regions appearing on the bifurcation diagram is not included here, but it may be found in [19]. In turn, system phase portraits of some key situations occurring in anaerobic digestion are presented and discussed.

The paper is organized as follows: Section 2 introduces the anaerobic digestion model while Section 3 details the calculation of the steady states. One-parameter diagrams, which show the magnitude of the system states and the amount of biogas produced along the equilibria branches are also provided. A comparison of the diagrams obtained using continuation software and the ones developed from the analytical expressions of equilibrium points is also included. The procedure to construct the two-parameters bifurcation diagram for the anaerobic digestion model is presented in Section 4. System phase portraits of representative operation conditions are shown in Section 5. Section 6 presents the generalization of the methodology for arbitrary order continuous stirred bioreactors. Conclusions are drawn in the last Section.

2. Model description

The model studied throughout this paper includes three stages of the anaerobic digestion process [17, 18], acidogenesis, acetogenesis and methanogenesis, and involves four nutrient groups and the corresponding bacterial groups: simple substrates S, volatile fatty acids (except of acetic acid) V, acetic acid A, hydrogen H, acidogenic bacteria X_S, acetogenic bacteria X_V, acetoclastic methanogens X_A and hydrogenotrophic methanogens X_H. It is assumed that the biomass decay is negligible and it is not included in the model equations. The model has the general structure

$$\dot{\xi} = D(\xi_{in} - \xi) + Kr(\xi) \tag{1}$$

where D is the dilution rate representing the influent flow scaled by the reactor volume, ξ is the state vector made of concentrations of components in the reactor, ξ_{in} is the vector of inlet concentrations, K is the matrix of stoichiometric coefficients and $r(\xi)$ represents the vector of reaction rates.The model is based on the

reaction network

$$k_1 S \xrightarrow{g_S} k_2 V + k_4 A + k_7 H + X_S \tag{2}$$

$$k_3 V \xrightarrow{g_V} k_5 A + k_8 H + X_V \tag{3}$$

$$k_6 A \xrightarrow{g_A} k_{10} CH_4 + X_A \tag{4}$$

$$k_9 H \xrightarrow{g_H} k_{11} CH_4 + X_H \tag{5}$$

The mass balances for each component read:

$$\frac{dX_S}{dt} = -DX_S + g_S(S)X_S \tag{6}$$

$$\frac{dX_V}{dt} = -DX_V + g_V(V,H)X_V \tag{7}$$

$$\frac{dX_A}{dt} = -DX_A + g_A(A)X_A \tag{8}$$

$$\frac{dX_H}{dt} = -DX_H + g_H(H,A)X_H \tag{9}$$

$$\frac{dS}{dt} = D(S_{in} - S) - k_1 g_S(S)X_S \tag{10}$$

$$\frac{dV}{dt} = -DV + k_2 g_S(S)X_S - k_3 g_V(V,H)X_V \tag{11}$$

$$\frac{dA}{dt} = -DA + k_4 g_S(S)X_S + k_5 g_V(V,H)X_V - k_6 g_A(A)X_A \tag{12}$$

$$\frac{dH}{dt} = -DH + k_7 g_S(S)X_S + k_8 g_V(V,H)X_V - k_9 g_H(H,A)X_H \tag{13}$$

while the rate of methane production is given by:

$$Q_M = k_{10} g_A(A)X_A + k_{11} g_H(H,A)X_H \tag{14}$$

In (6)- (14), S_{in} is the concentration of nutrient in the influent flow, k_i, $i = 1 \ldots 11$ are the stoichiometric parameters, while g_j, $j \in \{S, V, A, H\}$ denote the growth functions. The growth functions depend on the concentration of the component that is decomposed and other factors that might inhibit the reaction. Further on,

we use the explicit forms of the growth functions:

$$g_S(S) = \frac{m_S S}{K_S + S} \tag{15}$$

$$g_V(V, H) = \frac{m_V V}{K_V + V + \mu_H H} \tag{16}$$

$$g_A(A) = \frac{m_A A}{K_A + A + A^2/K_I} \tag{17}$$

$$g_H(H, A) = \frac{m_H H}{K_H + H + \mu_A A} \tag{18}$$

where m_j and K_j, with $j \in \{S, V, A, H\}$ respectively denote the maximum growth rates and the half-saturation constants in the absence of inhibition; K_I is a coefficient describing the inhibition due to A on the growth of X_A; μ_H and μ_A are inhibition factors for the growth of X_V and X_H respectively due to H and A.

All solutions of (6)- (13) with nonnegative initial conditions remain nonnegative and are bounded [17, 18]. Further on, we make use explicitly of the mathematical expressions of the system growth functions to analytically compute and characterize the equilibria, which is particularly important in view of efficiently operating and controlling the anaerobic digestion process.

3. Characterization of the steady states

To simplify the computation and characterization of the system equilibria, we use a well-known canonical state transformation [20], which reduces the system dynamics to the so-called reaction manifold [21]. Let us consider the state transformation $\xi = [\ \xi_a \quad \xi_b\ ]' \mapsto x = [\ x_a \quad x_b\ ]'$, with $x_a = \xi_a = [\ X_S \quad X_V \quad X_A \quad X_H\ ]'$ and x_b given by

$$x_b = \begin{bmatrix} S + k_1 X_S \\ V - k_2 X_S + k_3 X_V \\ A - k_4 X_S - k_5 X_V + k_6 X_A \\ H - k_7 X_S - k_8 X_V + k_9 X_H \end{bmatrix} \tag{19}$$

The state equations are rewritten as:

$$\dot{x}_1 = \frac{dX_S}{dt} = -Dx_1 + g_S(S)x_1 \tag{20}$$
$$\dot{x}_2 = \frac{dX_V}{dt} = -Dx_2 + g_V(V,H)x_2 \tag{21}$$
$$\dot{x}_3 = \frac{dX_A}{dt} = -Dx_3 + g_A(A)x_3 \tag{22}$$
$$\dot{x}_4 = \frac{dX_H}{dt} = -Dx_4 + g_H(H,A)x_4 \tag{23}$$
$$\dot{x}_5 = D(S_{in} - x_5) \tag{24}$$
$$\dot{x}_6 = -Dx_6 \tag{25}$$
$$\dot{x}_7 = -Dx_7 \tag{26}$$
$$\dot{x}_8 = -Dx_8 \tag{27}$$

The system dynamics converges to the space

$$S_x = \left\{ x \in \mathbb{R}^8 \,|x_i \geq 0, i = 1, \ldots, 4, x_5 = S_{in}, x_j = 0, j = 6, \ldots, 8 \right\} \tag{28}$$

All system equilibria lie in S_x, which implies that at equilibrium:

$$S + k_1 X_S = S_{in} \tag{29}$$
$$V - k_2 X_S + k_3 X_V = 0 \tag{30}$$
$$A - k_4 X_S - k_5 X_V + k_6 X_A = 0 \tag{31}$$
$$H - k_7 X_S - k_8 X_V + k_9 X_H = 0 \tag{32}$$

The system steady states are the solutions of

$$(-D + g_S(S)) \cdot x_1 = 0 \tag{33}$$
$$(-D + g_V(V,H)) \cdot x_2 = 0 \tag{34}$$
$$(-D + g_A(A)) \cdot x_3 = 0 \tag{35}$$
$$(-D + g_H(H,A)) \cdot x_4 = 0 \tag{36}$$
$$\tag{37}$$

Equations (33)-(36) lead to several possibilities detailed in Appendix A. Note that from a practical point of view, we are interested in the physical steady states, characterized by nonnegative values of all state components. Therefore the conditions for physical steady states are derived by requiring that $\bar{\xi}_i \geq 0$, $i = 1, \ldots, 8$,

where $\bar{\xi}_i$ denotes the value of state ξ_i at equilibrium. These conditions and the analytical expressions of the equilibria are summarized in Table 1. A classification of the equilibrium points can be achieved using the criteria listed below:

Total wash-out - one equilibrium point, always occurring
$\xi^W: \quad X_S = 0, X_V = 0, X_A = 0, X_H = 0$ - Case 1 in Appendix A

Wash-out of three microbial populations - one equilibrium point
$\xi^0: \quad X_V = 0, X_A = 0, X_H = 0$ - Case 2 in Appendix A

Wash-out of two microbial populations - up to four equilibrium points

- Wash-out of both methanogenic microorganisms
  $\xi^V: \quad X_A = 0, X_H = 0$ - Case 3 in Appendix A
- Wash-out of the acetogenic bacteria and acetoclastic methanogens
  $\xi^H: \quad X_V = 0, X_A = 0$ - Case 5 in Appendix A
- Wash-out of acetogenic bacteria and hydrogenotrophic methanogens
  $\xi_i^A, i = 1, 2: \quad X_V = 0, X_H = 0$ - Case 8 in Appendix A

Wash-out of one microbial population - up to five equilibrium points

- Wash-out of the acetogenic bacteria
  $\xi_i^{AH}, i = 1, 2: \quad X_H = 0$ - Case 7 in Appendix A
- Wash-out of acetoclastic methanogens
  $\xi^{VH}: \quad X_A = 0$ - Case 6 in Appendix A
- Wash-out of hydrogenotrophic methanogens
  $\xi_i^{VA}, i = 1, 2: \quad X_H = 0$ - Case 4 in Appendix A

Coexistence of all the species - up to two equilibrium points
$\xi_i^{VAH}, i = 1, 2$ - Case 9 in Appendix A

Table 2 shows the numerical values of the system parameters [18] employed for the simulation results, while Table 3 gives an overview of the physical equilibrium points which occur for a fixed inlet substrate concentration $S_{in} = 40$ COD/L and various values of the dilution rate. At low and medium dilution rate values a significant number of steady states occur, which also include the desirable equilibria ξ_i^{VAH}. At higher dilution rate values only steady states characterized by the wash-out of one or more microorganisms populations occur. The number of physical steady states can be also determined from the bifurcation diagram shown in

Table 1: Analytical expressions and conditions for occurrence of the equilibria

Equilibrium	Expression	Conditions
ξ^W	$\bar{X}_S = 0, \bar{X}_V = 0, \bar{X}_A = 0, \bar{X}_H = 0$	-
	$\bar{S} = S_{in}, \bar{V} = 0, \bar{A} = 0, \bar{H} = 0$	
ξ^0	$\bar{X}_S = (S_{in} - \bar{S})/k_1, \bar{X}_V = 0, \bar{X}_A = 0, \bar{X}_H = 0$	$D < m_S$
	$\bar{S} = DK_S/(m_S - D), \bar{V} = k_2/k_1 \cdot (S_{in} - \bar{S})$	
	$\bar{A} = k_4/k_1 \cdot (S_{in} - \bar{S}), \bar{H} = k_7/k_1 \cdot (S_{in} - \bar{S})$	$\bar{S} \leq S_{in}$
ξ^V	$\bar{X}_S = (S_{in} - \bar{S})/k_1, \bar{X}_V = (k_2\bar{X}_S - \bar{V})/k_3, \bar{X}_A = 0, \bar{X}_H = 0$	$D < m_S, \bar{S} \leq S_{in}$
	$\bar{S} = DK_S/(m_S - D), \bar{V} = \dfrac{D(K_V + \mu_H \bar{H})}{(m_V - D)}, \bar{A} = k_4\bar{X}_S + k_5\bar{X}_V$	$D < m_V$
	$\bar{H} = \dfrac{\left(\frac{(k_3k_7+k_8k_2)}{k_3}\bar{X}_S - \frac{k_8}{k_3}\frac{DK_V}{(m_V-D)}\right)}{\left(1 + \frac{k_8}{k_3}\frac{D\mu_H}{(m_V-D)}\right)}$	$k_1/k_2 \cdot \bar{V} + \bar{S} \leq S_{in}$
ξ_i^{VA}	$\bar{X}_S = (S_{in} - \bar{S})/k_1, \bar{X}_V = (k_2\bar{X}_S - \bar{V})/k_3$	$D < m_S, \bar{S} \leq S_{in}$
	$\bar{X}_{A_i} = (k_4\bar{X}_S + k_5\bar{X}_V - A_i)/k_6, \bar{X}_H = 0$	$D < m_V, D < \max(g_A(A))$
	$\bar{S} = DK_S/(m_S - D), \bar{V} = \dfrac{D(K_V + \mu_H \bar{H})}{(m_V - D)}, \bar{A}_i$ from (A.15)	$k_1/k_2 \cdot \bar{V} + \bar{S} \leq S_{in}$
	$\bar{H} = \dfrac{\left(\frac{(k_3k_7+k_8k_2)}{k_3}\bar{X}_S - \frac{k_8}{k_3}\frac{DK_V}{(m_V-D)}\right)}{\left(1 + \frac{k_8}{k_3}\frac{D\mu_H}{(m_V-D)}\right)}$	$k_3c_1\bar{A}_i + k_5c_1\bar{V} + \bar{S} \leq S_{in}$
ξ^H	$\bar{X}_S = (S_{in} - \bar{S})/k_1, \bar{X}_V = 0, \bar{X}_A = 0$	$D < m_S, \bar{S} \leq S_{in}, D < m_H$
	$\bar{X}_H = (k_7\bar{X}_S - \bar{H})/k_9, \bar{S} = DK_S/(m_S - D), \bar{V} = k_2\bar{X}_S$	$k_1/k_7 \cdot \bar{H} + \bar{S} \leq S_{in}$
	$\bar{A} = k_4\bar{X}_S, \bar{H} = \dfrac{D(K_H + \mu_A k_4 \bar{X}_S)}{(m_H - D)}$	
ξ^{VH}	$\bar{X}_S = (S_{in} - \bar{S})/k_1, \bar{X}_V = (k_2\bar{X}_S - \bar{V})/k_3$	$D < m_S, \bar{S} \leq S_{in}$
	$\bar{X}_A = 0, \bar{X}_H = (k_7\bar{X}_S + k_8\bar{X}_V - \bar{H})/k_9$	$D < m_V, D < m_H$
	$\bar{S} = DK_S/(m_S - D), \bar{A} = k_4\bar{X}_S + k_5\bar{X}_V, \bar{H} = \dfrac{D(K_H + \mu_A\bar{A})}{(m_H - D)}$	$k_1/k_2 \cdot \bar{V} + \bar{S} \leq S_{in}$
	$\bar{V} = \dfrac{D\left(K_V(m_H - D) + \mu_H D\left(K_H + \mu_A \bar{X}_S \frac{(k_3k_4+k_5k_2)}{k_3}\right)\right)}{\left((m_V - D)(m_H - D) + \mu_H\mu_A D^2 \frac{k_5}{k_3}\right)}$	$k_3c_2\bar{H} + k_8c_2\bar{V} + \bar{S} \leq S_{in}$
ξ_i^{AH}	$\bar{X}_S = (S_{in} - \bar{S})/k_1, \bar{X}_V = 0$	$D < m_S, \bar{S} \leq S_{in}$
	$\bar{X}_{A_i} = (k_4\bar{X}_S - \bar{A}_i)/k_6, \bar{X}_H = (k_7\bar{X}_S - \bar{H}_i)/k_9$	$D < \max(g_A(A)), D < m_H$
	$\bar{S} = DK_S/(m_S - D), \bar{V} = k_2\bar{X}_S, \bar{A}_i$ from (A.15)	$k_1/k_4 \cdot \bar{A}_i + \bar{S} \leq S_{in}$
	$\bar{H}_i = D\dfrac{(K_H + \mu_A\bar{A}_i)}{(m_H - D)}$	$k_1/k_7 \cdot \bar{H}_i + \bar{S} \leq S_{in}$
ξ_i^A	$\bar{X}_S = (S_{in} - \bar{S})/k_1, \bar{X}_V = 0, \bar{X}_{A_i} = (k_4\bar{X}_S - \bar{A}_i)/k_6$	$D < m_S, \bar{S} \leq S_{in}$
	$\bar{X}_H = 0, \bar{S} = DK_S/(m_S - D), \bar{V} = k_2\bar{X}_S$	$D < \max(g_A(A))$
	$\bar{A}_i$ from (A.15), $\bar{H} = k_7\bar{X}_S$	$k_1/k_4 \cdot \bar{A}_i + \bar{S} \leq S_{in}$
ξ_i^{VAH}	$\bar{X}_S = (S_{in} - \bar{S})/k_1, \bar{X}_{V_i} = (k_2\bar{X}_S - \bar{V}_i)/k_3$	$D < m_S, \bar{S} \leq S_{in}$
	$\bar{X}_{A_i} = (k_4\bar{X}_S + k_5\bar{X}_{V_i} - \bar{A}_i)/k_6,$	$D < m_V, D < \max(g_A(A))$
	$\bar{X}_{H_i} = (k_7\bar{X}_S + k_8\bar{X}_{V_i} - \bar{H}_i)/k_9$	$D < m_H, k_1/k_2 \cdot \bar{V}_i + \bar{S} \leq S_{in}$
	$\bar{S} = DK_S/(m_S - D), \bar{V}_i = D\dfrac{(K_V + \mu_H\bar{H}_i)}{(m_V - D)}$	$k_3c_1\bar{A}_i + k_5c_1\bar{V}_i + \bar{S} \leq S_{in}$
	$\bar{A}_i$ from (A.15), $\bar{H}_i = D\dfrac{(K_H + \mu_A\bar{A}_i)}{(m_H - D)}$	$k_3c_2\bar{H}_i + k_8c_2\bar{V}_i + \bar{S} \leq S_{in}$

Table 2: Numerical values for system parameters

Parameter	Value	Parameter	Value
m_S	3.5 day^{-1}	k_1	11.111
K_S	0.4 g COD/L	k_2	1.962
m_V	0.86 day^{-1}	k_3	20
K_V	0.3 g COD/L	k_4	6.419
m_A	0.4 day^{-1}	k_5	10.357
K_A	0.15 g COD/L	k_6	20
K_i	10 g COD/L	k_7	2.367
μ_H	1 g COD/L	k_8	5.268
m_H	2.1 day^{-1}	k_9	16.667
K_H	2.5e-5 g COD/L	k_{10}	19
μ_A	5 g COD/L	k_{11}	15.667

Table 3: Physical steady states for various values of the dilution rate and fixed inlet concentration

Dilution rate	Physical equilibria
$D = 0.1$	ξ^0, ξ^V, ξ_1^{VA}, ξ^H, ξ^{VH}, ξ_1^{AH}, ξ_1^A, ξ_1^{VAH}
$D = 0.14$	ξ^0, ξ^V, $\xi_{1,2}^{VA}$, ξ^H, ξ^{VH}, $\xi_{1,2}^{AH}$, $\xi_{1,2}^A$, $\xi_{1,2}^{VAH}$
$D = 0.2$, $D = 0.3$	ξ^0, ξ^V, $\xi_{1,2}^{VA}$, $\xi_{1,2}^{AH}$, $\xi_{1,2}^A$, $\xi_{1,2}^{VAH}$
$D = 0.35$	ξ^0, ξ^V
$D = 0.4$	ξ^0

Figure 1. Note that in addition the total wash-out state ξ^W is also a steady state of the anaerobic digestion system.

A comparison between the equilibria branches computed numerically, employing the continuation software MatCONT [16], and the ones obtained from the implementation of the expressions and conditions in Table 1 is shown in Figure 1. The equilibria branches are computed for a inlet substrate concentration $S_{in} = 40$ g COD/L. The results are shown only for one state variable, ie. the hydrogen concentration, and the outflow rate of methane Q_M. The branches for a certain type of equilibrium point are shown with the same color and type of line. The bifurcation points are also indicated on the graphs. They are either branch points (denoted by BP) or limit points (denoted by LP). The analytically established results are identical to the numerically computed ones. The notation and the meaning of the bifurcation points are as follows:

- BP_1 - ξ^V ceases to exist for dilution rates higher than D^{BP_1} (the value of the dilution rate for which the branch point occurs). D^{BP_1} is the dilution rate for which $k1/k2\bar{V} + \bar{S} = S_{in}$;
- BP_2 - ξ_2^{VA} does not occur for dilution rates lower than D^{BP_2}. D^{BP_2} is calculated from $k_3c_1\bar{A}_i + k_5c_1\bar{V} + \bar{S} = S_{in}$;
- BP_3 - ξ^H ceases to exist for dilution rates higher than D^{BP_3}. D^{BP_3} is calculated from $k_1/k_7\bar{H} + \bar{S} = S_{in}$;
- BP_4 - ξ^{VH} ceases to exist for dilution rates higher than D^{BP_4}. D^{BP_4} is calculated from $k_3c_2\bar{H} + k_8c_2\bar{V} + \bar{S} = S_{in}$;
- BP_5 - ξ_2^{AH} does not occur for dilution rates lower than D^{BP_5}. D^{BP_5} is calculated from $k_1/k_4\bar{A}_i + \bar{S} = S_{in}$;
- BP_6 - ξ_2^{A} does not occur for dilution rates lower than D^{BP_6}. D^{BP_6} is calculated from $k_1/k_4\bar{A}_i + \bar{S} = S_{in}$;
- BP_7 - ξ_2^{VAH} does not occur for dilution rates lower than D^{BP_7}. D^{BP_7} is calculated from $k_3c_1\bar{A}_i + k_5c_1\bar{V} + \bar{S} = S_{in}$;
- LP_i, with $i = 1 \ldots 4$ - ξ^{VA}, ξ^{AH}, ξ^{A}, ξ^{VAH} do not occur for dilution rates higher than D^{LP_i} (note that all limit points occur for the same dilution rate value, which is $D^{LP_i} = \max(g_A)$).

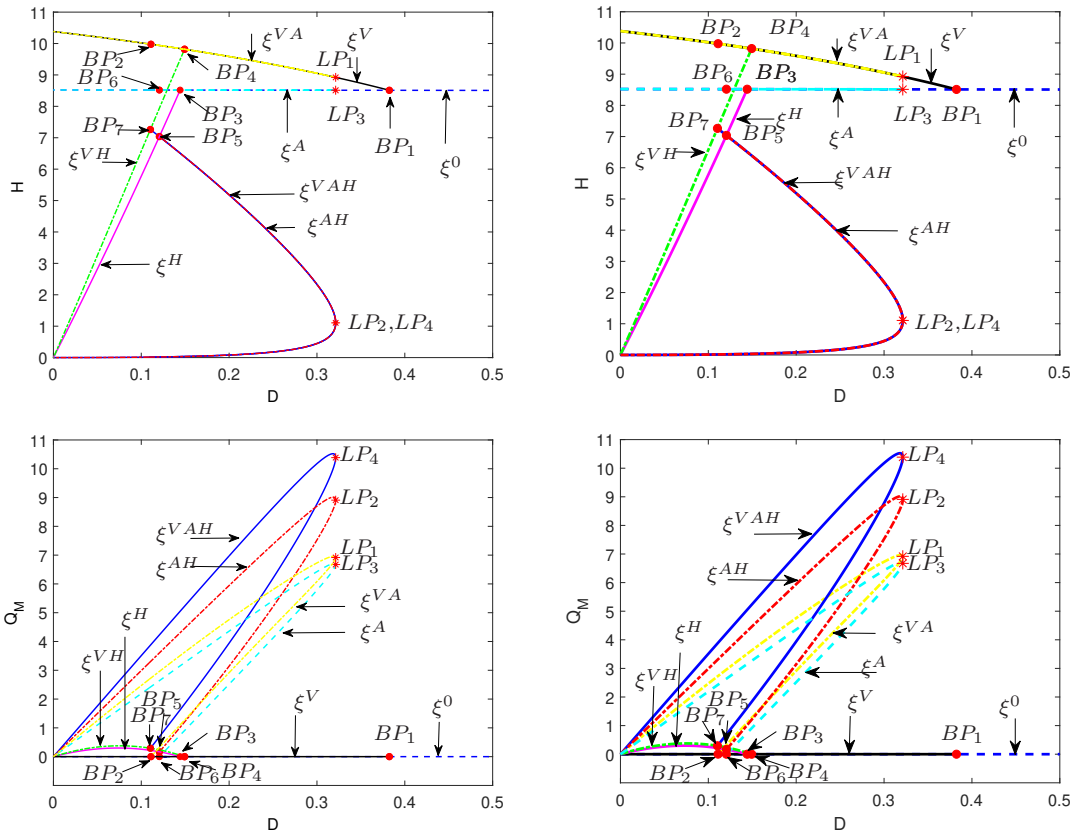

Figure 1: Comparison between the equilibria branches obtained numerically (first column) and analytically (second column)

4. Two-parameter bifurcation diagram

The analytic expression of equilibria can be used to draw one-parameter bifurcation diagrams for fixed substrate inlet concentration and variable dilution rate such as illustrated in Figure 1, which show how the magnitude of the system states changes with the varying dilution rate. This may allow to determine the type of the steady state characterized by maximum methane production and the magnitude of the dilution rate for which this maximum is reached. However it does not provide a global view on the steady state behavior of the system when the substrate inlet concentration varies, which is quite common in practice. If the organic load of the system undergoes modifications, not only the system efficiency is affected but also its stability. Therefore, the system operator may benefit from the availability of the two-parameter bifurcation diagram to keep the system operational. This diagram shows the regions in the input space (S_{in}, D) characterized by the occurrence of a certain type of steady state. Hence, when a change in the organic load occurs, the operator may consult this diagram and adjust the dilution rate accordingly to keep the system operating at the same type of steady state. In this section we develop the conditions necessary to build this diagram and provide the analytical expressions of the critical points.

The two-parameter bifurcation diagram is defined by the conditions for physical steady states summarized in the third column of Table 1. In other words, the bifurcation diagram shows how the branch points and limit points defined in Section 3 for a specific value of S_{in} change their location when S_{in} assumes different values in a certain range. While some of these conditions (eg. $D < m_S$) can be easily represented in the plane (S_{in}, D), the rest of them (those which are given in terms of the equilibrium values of the states) need further development as the dilution rate is an implicit parameter in the expression. The main idea behind the developments is to use the expressions of the states given in the second column of Table 1 in the boundary conditions (given in the third column of Table 1) and develop an equation which involves only the dilution rate D, the inlet substrate concentration S_{in} and the system parameters.

In Appendix B, we detail the reasoning for each type of conditional equilibrium point (all except for the total wash-out ξ^W). Note that the boundary between the regions of physical and non-physical equilibria is given by the equality expressed in the condition. To graphically illustrate these regions, as well as to simplify at some instants the calculation of the critical points, the numerical values for the system parameters given in Table 2 are used.

Figure 2 shows the bifurcation diagram of the anaerobic digestion model. For

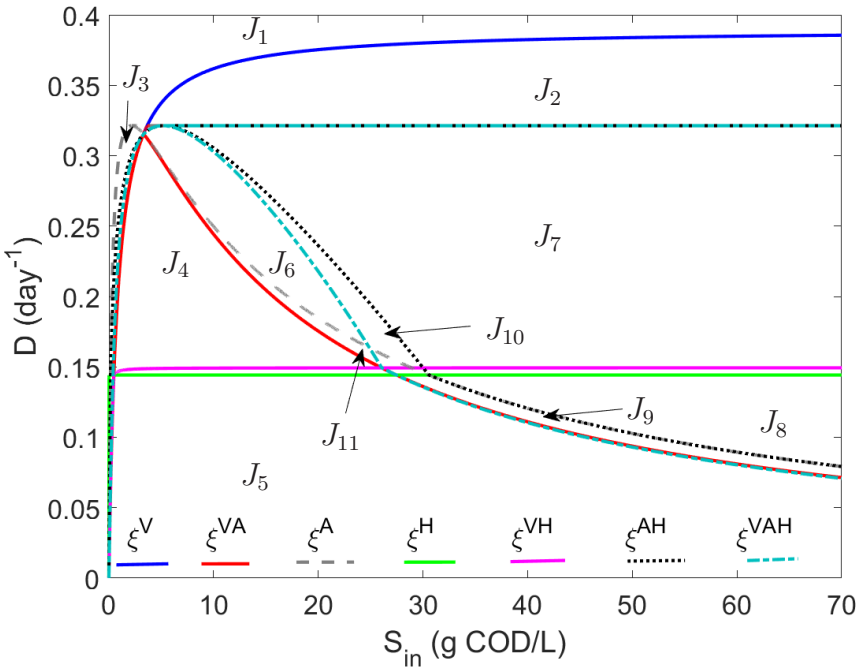

Figure 2: The bifurcation diagram

a better visibility, only the boundaries corresponding to the occurrence of the various equilibria are indicated on the graph, with different types of line and color. An overview of all equilibria, which occur in the regions indicated on the bifurcation diagram, is given in Table 4. Noticeably, the destabilization point of the process ξ^V, characterized by the accumulation of volatile fatty acids and no biogas production is a system equilibrium point for any reasonable operating choice of inputs. At lower dilution rate values, ξ^{VH} and ξ^H occur, characterized by a very low production of biogas, generated through the hydrogenotrophic methanogenesis. For dilution rates lower than $\max(g_A)$, ξ_1^{VA}, ξ_1^A, ξ_1^{AH} and ξ_1^{VAH} occur for almost any value of the substrate inlet concentration, while ξ_2^{VA}, ξ_2^A, ξ_2^{AH} and ξ_2^{VAH} occur for increasing dilution rate values and increasing substrate inlet concentrations. Biogas is produced in all these equilibria, either through acetoclastic methanogenesis or acetoclastic and hydrogenotrophic methanogenesis.

Table 4: The occurrence of the equilibrium points in the main regions of the bifurcation diagram: '-' - not physical, '+' - physical

	J_1	J_2	J_3	J_4	J_5	J_6	J_7	J_8	J_9	J_{10}	J_{11}
ξ^0	+	+	+	+	+	+	+	+	+	+	+
ξ^V	-	+	-	+	+	+	+	+	+	+	+
ξ_1^{VA}	-	-	-	+	+	+	+	+	+	+	+
ξ_2^{VA}	-	-	-	-	-	+	+	+	+	+	+
ξ^H	-	-	-	-	+	-	-	+	+	-	-
ξ^{VH}	-	-	-	-	+	-	-	+	+	-	-
ξ_1^{AH}	-	-	-	+	+	+	+	+	+	+	+
ξ_2^{AH}	-	-	-	-	-	-	+	+	-	-	-
ξ_1^A	-	-	+	+	+	+	+	+	+	+	+
ξ_2^A	-	-	-	-	-	+	+	+	-	+	-
ξ_1^{VAH}	-	-	-	+	+	+	+	+	+	+	+
ξ_2^{VAH}	-	-	-	-	-	-	+	+	+	+	-

5. Stability of equilibria and system phase portraits

The local stability of the steady states can be assessed by evaluating the eigenvalues of the Jacobian matrix at the specific equilibrium point. These computations are not included here to avoid a lengthy mathematical paper. A detailed stability analysis of all equilibrium points in the various regions of the bifurcation

diagram can be found in [19]. Here the emphasis is on the engineering aspects and on how the bifurcation diagram may be helpful for the system operation. Hence, the stability of the occurring equilibria is illustrated by means of system phase portraits in several operation points. The operation points are selected based on the bifurcation diagram to show various situations: i) low substrate inlet concentration, low dilution rate ($S_{in} = 15$g COD/L, $D = 0.12$day^{-1}); ii) low substrate inlet concentration, high dilution rate ($S_{in} = 15$g COD/L, $D = 0.25$day^{-1}); iii) high substrate inlet concentration, low dilution rate ($S_{in} = 50$g COD/L, $D = 0.12$day^{-1}); iv) high substrate inlet concentration, high dilution rate ($S_{in} = 50$g COD/L, $D = 0.20$day^{-1}).

Taking into account the high system dimensionality, and the fact that the system dynamics converges to the space S_x defined by (28), which contains all system equilibria, without loss of generality the phase portrait is restricted to the space S_x. Furthermore, note that except for the total wash-out condition ξ^W, all steady states lie on the hyperplane $x_1 = \bar{X}_S$. Thus, a three dimensional representation of the phase portrait on the hyperspace $S_x \cap (x_1 = \bar{X}_S)$ can be obtained.

In accordance with the practice, where biomass is produced only if it is initially present in the bioreactor or it is subsequently supplied with the influent (situation which is not characterized by the model (6)- (13)), the sets $x_2 = 0$, $x_3 = 0$, and $x_4 = 0$ ($X_V = 0$, $X_A = 0$, $X_H = 0$) are system invariants. Thus, a system trajectory starting in an initial condition in one of these sets, stays in the respective set for all future times. For a better visibility, each phase portrait is presented as a collection of two pictures. The picture on the top shows the phase portrait on the invariant sets, the system equilibria that lie on these sets and the physical boundaries. The physical boundaries represent the conditions when one state variable is zero. Note that some of these physical boundaries displayed in the figures correspond to state variables which are not explicitly shown in the pictures. These physical boundaries are given by:

$$\begin{aligned} V = 0: &\quad k_2 X_S - k_3 X_V = 0 \\ A = 0: &\quad k_4 X_S + k_5 X_V - k_6 X_H = 0 \\ H = 0: &\quad k_7 X_S + k_8 X_V - k_9 X_H = 0 \end{aligned} \tag{38}$$

The picture on the bottom shows all system equilibria and the phase portrait inside $S_x \cap (x_1 = \bar{X}_S)$.

Figure 3 shows the phase portrait when the system is operated with a low dilution rate and is characterized by low substrate inlet concentration. In this situation eight conditional equilibrium points occur, namely ξ^0, ξ^V, ξ^H, ξ^{VH}, ξ_1^A, ξ_1^{VA}, ξ_1^{AH}

and ξ_1^{VAH}. Note that due to the system parameters and operational conditions the equilibria ξ_1^{VA} and ξ_1^{AH} are situated close to the physical boundaries. Trajectories starting in initial conditions lying on the boundary $X_V = 0$, $X_H = 0$ converge to ξ_1^A, those starting in initial conditions lying on the boundary $X_A = 0$, $X_H = 0$ converge to ξ^V and those starting in initial conditions lying on the boundary $X_V = 0$, $X_A = 0$ converge to ξ^H. On the invariant set $X_V = 0$, all trajectories converge to ξ_1^{AH}. On the invariant set $X_A = 0$, all trajectories converge to ξ^{VH}. On the invariant set $X_H = 0$, all trajectories converge to ξ_1^{VA}. All trajectories starting in initial conditions characterized by the presence of all types of biomass converge to the steady state ξ_1^{VAH}. Note that operating the system with low dilution rate and low inlet concentration is safe in the sense that the system preserves its stability properties and treatment ability (no biomass is washed out, thus all transformations occurring initially will further occur). Some amount of biogas is produced in all equilibria except of ξ^0 and ξ^V. However, the system efficiency is low. Operating the system with low dilution rate may be appropriate for system start-up, but it does not represent a long term solution. High system efficiency requires high dilution rate.

When the dilution rate increases, the bistability feature, which characterizes the bioreactor systems with inhibition occurs. Figure 4 shows the consequences on the phase portrait of an increased dilution rate. The same number of physical equilibrium points occurs for this choice of dilution rate and inlet concentration: ξ^0, ξ^V, $\xi_{1,2}^A$, $\xi_{1,2}^{VA}$, ξ_1^{AH} and ξ_1^{VAH}. Thus, ξ^H and ξ^{VH}, which occur at low dilution rate values are replaced by ξ_2^A and ξ_2^{VA}, which occur only at higher dilution rate values. Now trajectories starting in initial conditions on the boundary $X_V = 0$, $X_H = 0$ converge either to ξ_1^A or ξ^0 depending on whether the initial concentration of acetoclastic methanogens is higher or smaller than the concentration of acetoclastic methanogens at the equilibrium ξ_2^A. On the invariant set $X_V = 0$ trajectories converge either to ξ_1^{AH} or ξ^0 depending on the initial condition. Similarly, on the invariant set $X_H = 0$ trajectories converge either to ξ_1^{VA} or ξ^V, while on the invariant set $X_A = 0$ all trajectories converge to ξ^V. Now the trajectories starting in initial conditions in the interior set $(S_x \cap (x_1 = \bar{X}_S))$ converge either to ξ_1^{VAH} or ξ^V. It becomes now clear that even if increased efficiency may be achieved by operating the system with high dilution rate, this is not a trivial task to perform as the system dynamics may settle down in an undesirable equilibrium point.

Another feature of anaerobic digestion systems that require particular attention is the overload situation, when the influent characteristics change and high substrate inlet concentrations are supplied to the system. When such an overload

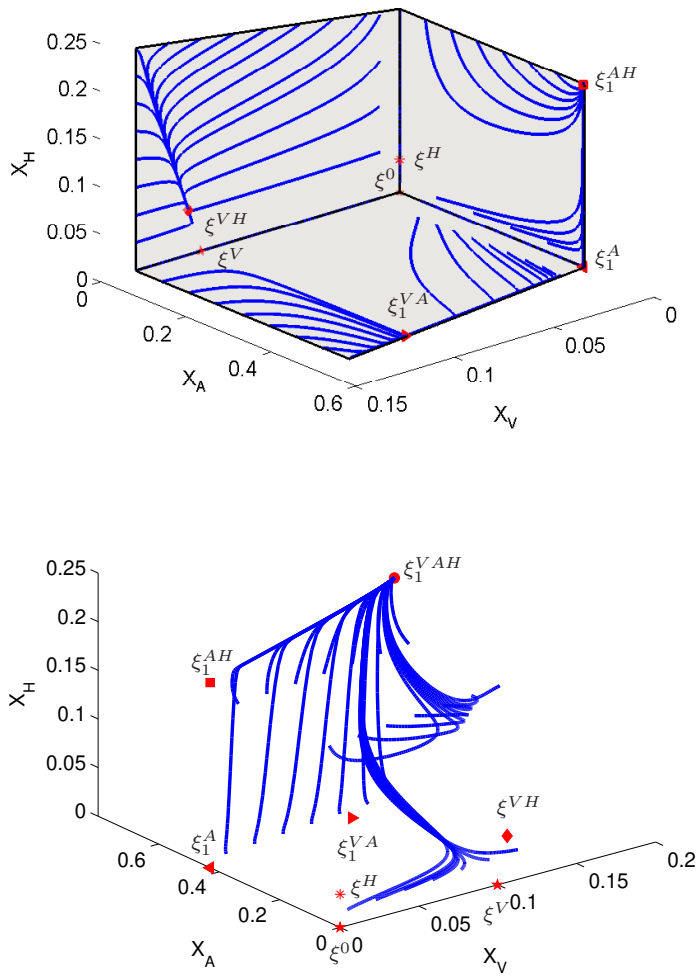

Figure 3: The system phase portrait for $S_{in} = 15$g COD/L, $D = 0.12\text{day}^{-1}$

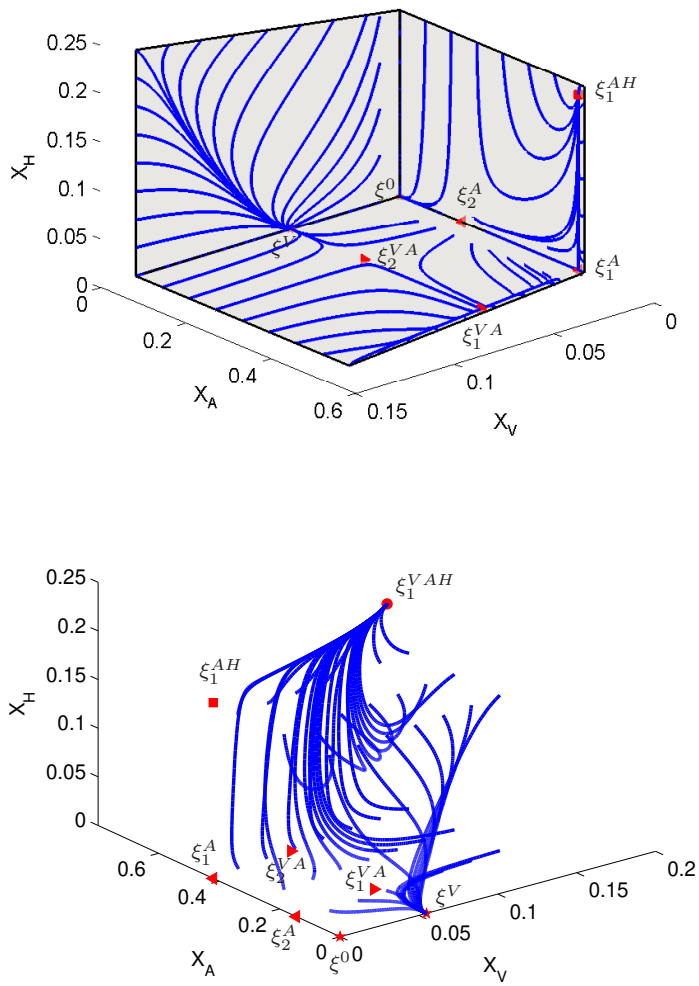

Figure 4: The system phase portrait for $S_{in} = 15$g COD/L, $D = 0.25\text{day}^{-1}$

occurs during the operation with a low dilution rate, the system phase portrait changes to the one illustrated in Figure 5. Twelve equilibrium points occur: ξ^0, ξ^V, ξ^H, ξ^{VH}, $\xi^A_{1,2}$, $\xi^{VA}_{1,2}$, $\xi^{AH}_{1,2}$ and $\xi^{VAH}_{1,2}$. On the physical boundary $X_V = 0$, $X_H = 0$, trajectories converge either to ξ^A_1 or ξ^0. On the physical boundary $X_A = 0$, $X_H = 0$, all trajectories converge to ξ^V. On the invariant set $X_V = 0$, trajectories converge either to ξ^{AH}_1 or ξ^H. On the invariant set $X_H = 0$, trajectories converge either to ξ^{VA}_1 or ξ^V, while on the invariant set $X_A = 0$ all trajectories converge to ξ^{VH}. Trajectories starting in initial conditions lying in the interior set $(S_x \cap (x_1 = \bar{X}_S))$ converge either to ξ^{VAH}_1 or ξ^{VH}.

If the system is operated with a high dilution rate at high substrate inlet concentrations, the system phase portrait changes to the one shown in Figure 6. Ten equilibrium points occur in this situation: ξ^0, ξ^V, $\xi^A_{1,2}$, $\xi^{VA}_{1,2}$, $\xi^{AH}_{1,2}$ and $\xi^{VAH}_{1,2}$. As previously, trajectories on the physical boundary $X_V = 0$, $X_H = 0$ converge either to ξ^A_1 or ξ^0. Trajectories on the invariant set $X_V = 0$ converge either to ξ^{AH}_1 or ξ^0. Trajectories on the invariant set $X_H = 0$ converge either to ξ^{VA}_1 or ξ^V, while trajectories on the invariant set $X_A = 0$ converge to ξ^V. Initial conditions in the interior set lead to trajectories that converge either to the nominal equilibrium point ξ^{VAH}_1 or to the destabilization point ξ^V. It is evident from the presented phase portraits that increasing the dilution rate enlarges the attraction region of the acidification point ξ^V, where volatile fatty acids accumulate and are not further processed to acetic acid, while the attraction region of the nominal equilibrium shrinks, making the efficient operation of the system less manageable.

6. Summary of the methodology

To emphasize the applicability of this methodology to other bioprocesses, the main steps are briefly described below. Consider a bioprocess taking place in a continuous stirred tank reactor, characterized by n components involved in m biochemical reactions (with $m < n$), whose dynamics is given by (1).

Step #1 Rewrite the model in canonical form: this has the advantage that the system is rewritten as nonlinear dynamics of dimension m coupled with linear dynamics of dimension $n - m$. To this end consider the state transformation $\xi = [\ \xi_a \quad \xi_b\ ]' \mapsto x = [\ x_a \quad x_b\ ]'$, with $x_a = \xi_a \in \mathbb{R}^{+m}$ and $x_b = -K_b K_a^{-1} \xi_a + \xi_b \in \mathbb{R}^{(n-m)}$ and $K_a \in \mathbb{R}^{m \times m}$, $K_b \in \mathbb{R}^{(n-m) \times m}$ the respective partitions of the stoichiometric coefficients matrix K. Without loss of generality, assume that the system equations are ordered such that ξ_a represent the microorganism populations involved in the process. This assumption brings some simplification in the nonlinear part of the canonical

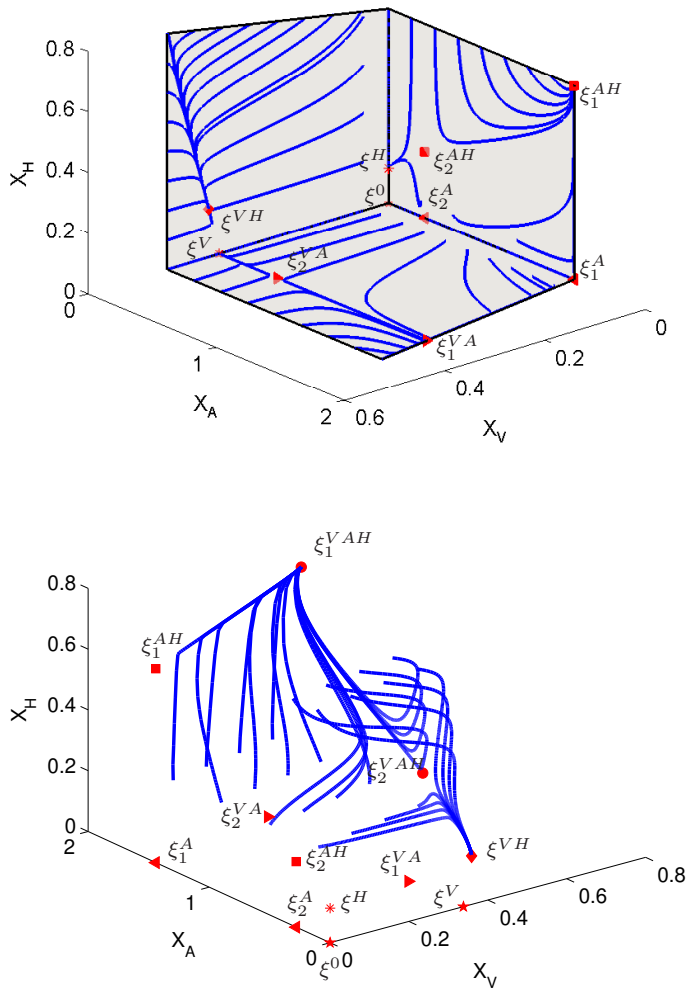

Figure 5: The system phase portrait for $S_{in} = 50$g COD/L, $D = 0.12\text{day}^{-1}$

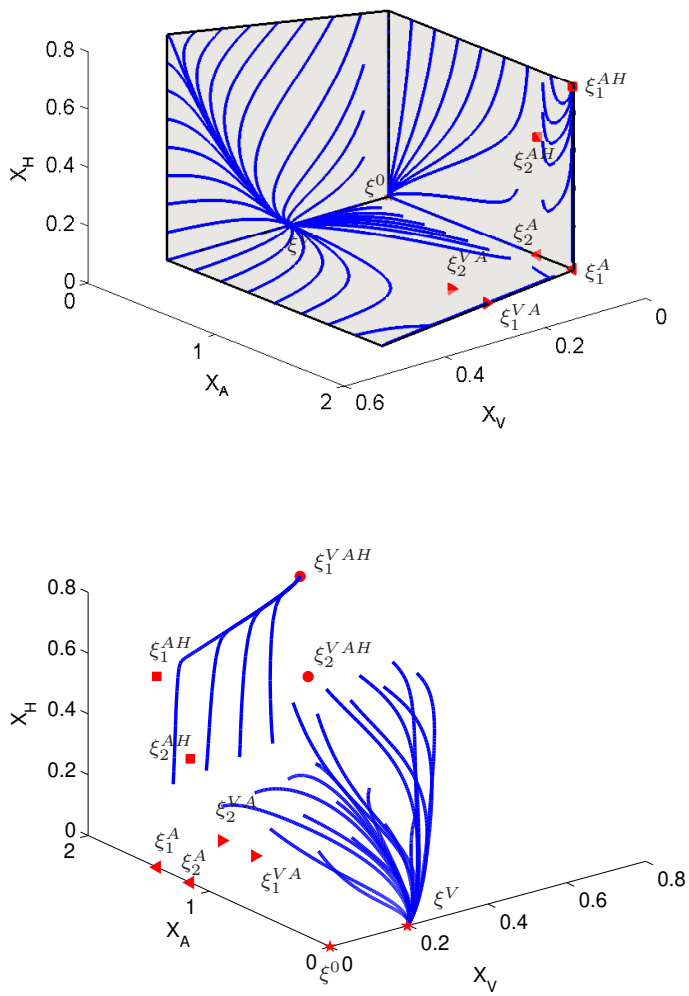

Figure 6: The system phase portrait for $S_{in} = 50$g COD/L, $D = 0.25$day^{-1}

representation as generally $K_a = I_m$, where I_m denotes the identity matrix of dimension m. Additionally, in many applications biomass is not supplied in the influent, therefore $\xi_{in,a} = 0$. Hence, the model is rewritten as

$$\dot{x}_i = (-D + \mu_i) \cdot x_i, \quad i = 1 \dots m \tag{39}$$

$$\dot{x}_j = D(\xi_{in,j} - x_j), \quad j = (m+1) \dots n \tag{40}$$

where μ_i, $i = 1 \dots m$ represent the growth functions.

Step #2 Identify the equations for computing the equilibria and determine an initial set of conditions for equilibria occurrence: the steady states are calculated by setting the derivatives to zero in (39), (40). The set of equations (40) provide the solutions $x_j = \xi_{in,j}$, $j = m+1 \dots n$. These are $n - m$ linear combinations of the original system states. The set of equations (39) leads to several possibilities that have to be investigated, since for each equation either $x_i = 0$ or $\mu_i = D$. The latter relationship provides also a condition for the occurrence of the steady state, as the equation will have a solution only if the dilution rate satisfies some condition, which generally can be expressed in terms of the maximum value or the limit value of the growth function μ_i, i.e.

$$D < \lim_{\xi_j \to +\infty} (\mu_i(\xi_j)) \tag{41}$$

$$D \leq \max(\mu_i(\xi_j)) \tag{42}$$

Further on, we will refer to the set of conditions of form (41) and/or (42) as conditions *C1*.

Step #3 Computation of the equilibria and statement of the conditions for physical steady states: all system equilibrium points are computed from the expressions identified in the previous step, by analyzing each possibility and recursively using the linear combination of the states provided by the second part of the canonical model. The number of the steady states will depend on the type of the kinetics. Monod type growth function leads to one steady state, Haldane type growth function leads to two steady states. Once the expression for each state at equilibrium has been established, $\bar{\xi} = \left[\bar{\xi}_1 \dots \bar{\xi}_n \right]'$, the equilibrium point is physical only if $\bar{\xi}_i \geq 0$, for all $i = 1 \dots n$. Further on, we will refer to these conditions as conditions *C2*.

Step #4 One-parameter bifurcation diagrams: based on the developments done in the previous steps, one can draw the one-parameter bifurcation diagrams, which illustrate the values of the system states along the equilibria branches. These are representations in the space (ξ_i, D) that are obtained as follows: i) for each type of equilibrium point the dilution rate is varied between 0 and the maximum value determined by the corresponding condition *C1*; ii) for each defined value of the dilution rate, the equilibrium point is computed and the corresponding conditions *C2* are checked; iii) if the conditions *C2* are fulfilled, then the equilibrium point is physical and it can be represented on the diagrams. If at least one of the conditions *C2* is not fulfilled, the equilibrium point is not physical. In this case the algorithm continues by considering the next type of equilibrium point. The diagrams are complete when all equilibria have been investigated and the physical ones have been displayed.

Step #5 Two-parameters bifurcation diagrams: these are usually representations in the space $(\xi_{in,i}, D)$. When several components $\xi_{in,i}$ are present in the influent, it is however possible that the two-parameters diagrams for some of the system equilibria are represented in function of linear combinations of the inlet concentrations. These diagrams are constructed from the conditions *C1* and *C2* as follows. For each equilibrium point: i) conditions *C1* can be represented directly on the diagram as they express constraints on the dilution rate in function of the inlet concentrations; ii) conditions *C2* need further development before representation as they are given in terms of the system states at the steady state. To rewrite the conditions *C2* in a form that can be represented on the two-parameters bifurcation diagrams, one needs to employ the expressions of the states at equilibrium until a relationship between the dilution rate D and the inlet concentrations $\xi_{in,i}$ is obtained; iii) the intersections points between the various conditions need to be computed.

7. Conclusions

In this paper the analytical computation and the characterization of steady states for a complex model describing the anaerobic digestion process is presented. The analytical expressions of equilibria allow to determine not only the type of equilibria in which the anaerobic digestion system produces biogas, but also to classify these equilibria in terms of their productivity. Furthermore, one-parameter bifurcation diagrams (i.e. the dilution rate is varied while the inlet

substrate concentration is kept constant) for the system states and biogas may be easily obtained.

Since the system disturbance input, i.e. the substrate inlet concentration, plays an important role in the process and may lead to process instability in overload situations, a two-parameter bifurcation diagram is constructed to show the influence of the pair (S_{in}, D) on the system steady state behavior. The procedure employed to construct the diagram makes explicit use of the kinetics structure. Analytical expressions for all branches and for all critical points are provided. The main advantage of the technique is the low computational requirements and cost, as the construction of the bifurcation diagram involve only the solutions of algebraic equations, which can be easily obtained with widely available simulation software. The system complex behavior is illustrated by means of phase portraits.

References

[1] D. Wu, L. Li, X. Zhao, Y. Peng, P. Yang, X. Peng, Anaerobic digestion: A review on process monitoring, Renewable and Sustainable Energy Reviews 103 (2019) 1–12.

[2] C. Onwosi, I. Eke, V. Igbokwe, J. Odimba, J. Ndukwe, K. Chukwu, G. Aliyu, T. Nwagu, Towards effective management of digester dysfunction during anaerobic treatment processes, Renewable and Sustainable Energy Reviews 116 (2019) 109424.

[3] J. Jimenez, E. Latrille, J. Harmand, A. Robles, J. Ferrer, D. Gaida, C. Wolf, F. Mairet, O. Bernard, V. Alcaraz-Gonzalez, H. Mendez-Acosta, D. Zitomer, D. Totzke, H. Spanjers, F. Jacobi, A. Guwy, R. Dinsdale, G. Premier, S. Mazhegrane, G. Ruiz-Filippi, A. Seco, T. Ribeiro, A. Pauss, J.-P. Steyer, Instrumentation and control of anaerobic digestion processes: a review and some research challenges, Reviews in Environmental Science and Bio/Technology 14 (2015) 615–648.

[4] D. Gaida, C. Wolf, M. Bongards, Feed control of anaerobic digestion processes for renewable energy production: A review, Renewable and Sustainable Energy Reviews 68 (2017) 869–875.

[5] D. J. Batstone, J. Keller, I. Angelidaki, S. V. Kalyuzhnyi, S. G. Pavlostathis, A. Rozzi, V. A. Vavilin, The IWA Anaerobic Digestion Model No 1(ADM 1), IWA Publishing, London, 2002.

[6] A. Bornhöft, R. Hanke-Rauschenbach, K. Sundmacher, Steady-state analysis of the anaerobic digestion model no. 1 (ADM1), Nonlinear Dynamics 73 (2013) 535–549.

[7] S. Shen, G. Premier, A. Guwy, R. Dinsdale, Bifurcation and stability analysis of an anaerobic digestion model, Nonlinear Dynamics 48 (2007) 391–408.

[8] J. Hess, O. Bernard, Design and study of a risk management criterion for an unstable anaerobic wastewater treatment process, Journal of Process Control 18 (2008) 71–79.

[9] M. Sbarciog, M. Loccufier, E. Noldus, Determination of appropriate operating strategies for anaerobic digestion systems, Biochemical Engineering Journal 51 (2010) 180–188.

[10] M. Sbarciog, M. Loccufier, E. Noldus, The estimation of stability boundaries for an anaerobic digestion system, in: Computer Applications in Biotechnology 11, Leuven, Belgium, 2010, pp. 330–335.

[11] B. Benyahia, T. Sari, B. Cherki, J. Harmand, Bifurcation and stability analysis of a two step model for monitoring anaerobic digestion processes, Journal of Process Control 22 (2012) 1008–1019.

[12] A. Rincón, J. Villa, F. Angulo, G. Olivar, A dynamic analysis for an anaerobic digester: Stability and bifurcation branches, Mathematical Problems in Engineering 2014 (2014) Article ID 514797.

[13] R. Fekih-Salem, Y. Daoud, N. Abdellatif, T. Sari, A mathematical model of anaerobic digestion with syntrophic relationship, substrate inhibition and distinct removal rates, hal-02085693 (2019).

[14] Z. Khedim, B. Benyahia, B. Cherki, T. Sari, J. Harmand, Effect of control parameters on biogas production during the anaerobic digestion of protein-rich substrates, Applied Mathematical Modelling 61 (2018) 351–376.

[15] A. Alzate-Ibanez, C. Ocampo-Martinez, C. Cardona Alzate, V. Trejos Montoya, Risk index to monitor an anaerobic digester using a dynamic model based on dilution rate, temperature, and ph, Nonlinear Engineering 9 (2020) 35–50.

[16] A. Dhooge, W. Govaerts, Y. Kuznetsov, H. Meijer, B. Sautois, New features of the software matcont for bifurcation analysis of dynamical systems, Mathematical and Computer Modelling of Dynamical Systems 14 (2008) 147–175.

[17] M. Weedermann, G. Seo, G. Wolkowicz, Mathematical model of anaerobic digestion in a chemostat: effects of syntrophy and inhibition, journal of biological dynamics, Journal of Biological Dynamics 7 (2013) 59–85.

[18] M. Weedermann, G. Wolkowicz, J. Sasara, Optimal biogas production in a model for anaerobic digestion, Nonlinear Dynamics 81 (2015) 1097–1112.

[19] M. Sbarciog, A. Vande Wouwer, J. Van Impe, L. Dewasme, Extremum seeking control of a three-stage anaerobic digestion model, in: IFAC World Congress, Berlin, Germany, 2020.

[20] G. Bastin, D. Dochain, On-line estimation and adaptive control of bioreactors, Elsevier, Amsterdam, 1990.

[21] K. Stamatelatou, L. Syrou, C. Kravaris, G. Lyberatos, An invariant manifold approach for cstr model reduction in the presence of multi-step biochemical reaction schemes. application to anaerobic digestion, Chemical Engineering Journal 150 (2009) 462–475.

Appendix A. Calculation of the steady states

1. $x_1 = 0$ ($X_S = 0$): In this case, the only physical equilibrium of the system is the total wash-out state, where no conversion takes place. This steady state occurs independently of the dilution rate D and the concentration of substrate in the influent S_{in}. In canonical coordinates and physical states respectively, the total wash-out steady state is given by:

$$x^W = \begin{bmatrix} 0 & 0 & 0 & 0 & S_{in} & 0 & 0 & 0 \end{bmatrix}'$$

$$\xi^W = \begin{bmatrix} 0 & 0 & 0 & 0 & S_{in} & 0 & 0 & 0 \end{bmatrix}'$$

2. $g_S(S) = D$, $x_2 = x_3 = x_4 = 0$ ($X_V = X_A = X_H = 0$): This steady state is characterized by the degradation of the organic substrate and the wash-out of the acetogenic bacteria, acetoclastic methanogens and hydrogenotrophic methanogens. The equation $g_S(S) = D$ has only one solution

$$\bar{S} = DK_S/(m_S - D) \tag{A.1}$$

According to (29)-(32),

$$\bar{X}_S = 1/k_1 \cdot (S_{in} - \bar{S}) \tag{A.2}$$
$$\bar{V} = k_2/k_1 \cdot (S_{in} - \bar{S}) \tag{A.3}$$
$$\bar{A} = k_4/k_1 \cdot (S_{in} - \bar{S}) \tag{A.4}$$
$$\bar{H} = k_7/k_1 \cdot (S_{in} - \bar{S}) \tag{A.5}$$

The equilibrium point

$$x^0 = \begin{bmatrix} \bar{X}_S & 0 & 0 & 0 & S_{in} & 0 & 0 & 0 \end{bmatrix}'$$

$$\xi^0 = \begin{bmatrix} \bar{X}_S & 0 & 0 & 0 & \bar{S} & \bar{V} & \bar{A} & \bar{H} \end{bmatrix}'$$

is a physical equilibrium point if and only if (A.1)-(A.5) are nonnegative, which imply that

$$D < m_S \tag{A.6}$$
$$\bar{S} \leq S_{in} \tag{A.7}$$

Note that the equation $g_S(S) = D$ is involved in the calculation of all subsequent equilibria. Hence, in these steady states the concentration of organic substrate $\bar{S}$ and the concentration of the acidogenic bacteria $\bar{X}_S$ are respectively given by (A.1) and (A.2). Consequently the conditions (A.6), (A.7) must hold for all the subsequently calculated steady states.

3. $g_S(S) = D$, $g_V(V, H) = D$, $x_3 = x_4 = 0$ ($X_A = X_H = 0$): This steady state is characterized by the conversion of the organic substrate and volatile fatty acids, and accumulation of acetic acid and hydrogen as no conversion of these substrates into biogas takes place due to the wash-out of the methanogenic microorganisms. The equation $g_V(V, H) = D$ has only one solution

$$\bar{V} = D(K_V + \mu_H \bar{H})/(m_V - D) \tag{A.8}$$

while (30)- (32) lead to:

$$\bar{X}_V = 1/k_3(k_2 \bar{X}_S - \bar{V}) \tag{A.9}$$
$$\bar{A} = k_4 \bar{X}_S + k_5 \bar{X}_V \tag{A.10}$$
$$\bar{H} = k_7 \bar{X}_S + k_8 \bar{X}_V \tag{A.11}$$

Under the conditions $\bar{X}_S \geq 0$ and $\bar{X}_V \geq 0$, (A.10) and (A.11) imply that the concentrations of acetic acid $\bar{A}$ and of hydrogen $\bar{H}$ are positive. The

concentration of volatile fatty acids $\bar{V}$ given by (A.8) is positive if and only if

$$D < m_V \tag{A.12}$$

The concentration of substrate $\bar{S}$ and acidogenic bacteria $\bar{X}_S$ are positive if (A.6) and (A.7) hold. The concentration of the acetogenic bacteria $\bar{X}_V$ is nonnegative if and only if

$$k_1/k_2 \cdot \bar{V} + \bar{S} \leq S_{in} \tag{A.13}$$

which results from using (A.2) in (A.9). The corresponding steady state

$$x^V = \begin{bmatrix} \bar{X}_S & \bar{X}_V & 0 & 0 & S_{in} & 0 & 0 & 0 \end{bmatrix}'$$

$$\xi^V = \begin{bmatrix} \bar{X}_S & \bar{X}_V & 0 & 0 & \bar{S} & \bar{V} & \bar{A} & \bar{H} \end{bmatrix}'$$

is characterized by the conversion of the substrate into VFAs which are further processed to acetic acid. Since none of the methanogens are present in the reactor, no methane production occurs.

4. $g_S(S) = D$, $g_V(V, H) = D$, $g_A(A) = D$, $x_4 = 0$ ($X_H = 0$): This type of steady state is characterized by the conversion of organic substrate, volatile fatty acids and acetic acid. Methane is only produced through acetoclastic methanogenesis, as the hydrogenotrophic methanogens are washed out. The equation $g_A(A) = D$ has two real solutions $\bar{A}_i$, $i = 1, 2$, with $\bar{A}_1 < \bar{A}_2$ if

$$D < \max(g_A(A)) = g_A(\sqrt{K_A K_I}) \tag{A.14}$$

Rewriting $g_A(A) = D$ as

$$A^2 + K_I \frac{(D - m_A)}{D} A + K_A K_I = 0 \tag{A.15}$$

one may find the solutions $\bar{A}_i$, $i = 1, 2$ as

$$\bar{A}_i = \frac{1}{2} \left(\frac{K_I(m_A - D)}{D} \mp \sqrt{\left(\frac{K_I(D - m_A)}{D} \right)^2 - 4K_A K_I} \right) \tag{A.16}$$

There may be up to two equilibria of this type

$$x_i^{VA} = \begin{bmatrix} \bar{X}_S & \bar{X}_V & \bar{X}_{A_i} & 0 & S_{in} & 0 & 0 & 0 \end{bmatrix}'$$

$$\xi_i^{VA} = \left[\begin{array}{cccccccc} \bar{X}_S & \bar{X}_V & \bar{X}_{A_i} & 0 & \bar{S} & \bar{V} & \bar{A}_i & \bar{H} \end{array}\right]'$$

where $\bar{X}_S$ and $\bar{S}$ are respectively given by (A.2), (A.1), $\bar{X}_V$ and $\bar{V}$ are respectively given by (A.9), (A.8), while $\bar{X}_{A_i}$ and $\bar{H}$ follow from (31), (32) as:

$$\bar{X}_{A_i} = 1/k_6(k_4\bar{X}_S + k_5\bar{X}_V - \bar{A}_i) \tag{A.17}$$

$$\bar{H} = k_7\bar{X}_S + k_8\bar{X}_V \tag{A.18}$$

Provided that $\bar{X}_S$ and $\bar{X}_V$ are positive, which means that (A.6), (A.7), (A.12), (A.13) are fulfilled, (A.18) ensures that the hydrogen concentration is positive. The concentrations of acetoclastic methanogens $\bar{X}_{A_i}$ are nonnegative if and only if

$$k_3c_1\bar{A}_i + k_5c_1\bar{V} + \bar{S} \leq S_{in} \tag{A.19}$$

with $c_1 = k_1/(k_3k_4 + k_5k_2)$. This condition is derived by using (A.2) and (A.9) in (A.17). The steady states ξ_i^{VA} are characterized by methane production.

5. $g_S(S) = D$, $x_2 = x_3 = 0$ ($X_V = X_A = 0$), $g_H(H, A) = D$: This steady state is characterized by the wash-out of the acetogenic bacteria and acetoclastic methanogens but some methane production is ensured by the presence of the hydrogenotrophic methanogens. The equation $g_H(H, A) = D$ has one positive solution

$$\bar{H} = \frac{D}{(m_H - D)}(K_H + \mu_A\bar{A}) \tag{A.20}$$

According to (30)- (32)

$$\bar{V} = k_2\bar{X}_S \tag{A.21}$$

$$\bar{A} = k_4\bar{X}_S \tag{A.22}$$

$$\bar{X}_H = 1/k_9 \cdot (k_7\bar{X}_S - \bar{H}) \tag{A.23}$$

The equilibrium

$$x^H = \left[\begin{array}{cccccccc} \bar{X}_S & 0 & 0 & \bar{X}_H & S_{in} & 0 & 0 & 0 \end{array}\right]'$$

$$\xi^H = \left[\begin{array}{cccccccc} \bar{X}_S & 0 & 0 & \bar{X}_H & \bar{S} & \bar{V} & \bar{A} & \bar{H} \end{array}\right]'$$

is physical if (A.6), (A.7) hold simultaneously with

$$D < m_H \tag{A.24}$$

$$k_1/k_7 \cdot \bar{H} + \bar{S} \leq S_{in} \tag{A.25}$$

which respectively result from $\bar{H} > 0$ and $\bar{X}_H \geq 0$.

6. $g_S(S) = D$, $g_V(V,H) = D$, $X_A = 0$, $g_H(H,A) = D$: This possibility leads to the equilibrium point

$$x^{VH} = \left[\begin{array}{cccccccc} \bar{X}_S & \bar{X}_V & 0 & \bar{X}_H & S_{in} & 0 & 0 & 0 \end{array}\right]'$$

$$\xi^{VH} = \left[\begin{array}{cccccccc} \bar{X}_S & \bar{X}_V & 0 & \bar{X}_H & \bar{S} & \bar{V} & \bar{A} & \bar{H} \end{array}\right]'$$

which is characterized by organic substrate, volatile fatty acids and hydrogen conversions. Methane generation is ensured by the presence of hydrogenotrophic methanogens $\bar{X}_H$. In this steady state, the concentrations of acidogenic bacteria $\bar{X}_S$ and organic substrate $\bar{S}$ are respectively given by (A.2) and (A.1), while the concentrations of acetogenic bacteria $\bar{X}_V$, volatile fatty acids $\bar{V}$ and hydrogen $\bar{H}$ are respectively calculated with (A.9), (A.8) and (A.20). The rest of the states in ξ^{VH} are further computed from (31), (32) as

$$\bar{A} = k_4\bar{X}_S + k_5\bar{X}_V \tag{A.26}$$

$$\bar{X}_H = 1/k_9 \cdot \left(k_7\bar{X}_S + k_8\bar{X}_V - \bar{H}\right) \tag{A.27}$$

To be a physical steady state (A.6), (A.7) and (A.12) (A.13), (A.24) must hold and additionally

$$k_3c_2\bar{H} + k_8c_2\bar{V} + \bar{S} \leq S_{in} \tag{A.28}$$

with $c_2 = k_1/(k_3k_7 + k_8k_2)$. Relationship (A.28) is derived from the condition $\bar{X}_H \geq 0$.

7. $g_S(S) = D$, $X_V = 0$, $g_A(A) = D$, $g_H(H,A) = D$: In this type of steady state conversions of organic substrate, acetic acid and hydrogen take place. Methane is generated through both acetoclastic and hydrogenotrophic methanogenesis. The equation $g_A(A) = D$ has two solutions if (A.14) holds, while $g_H(H,A) = D$ has one solution if (A.24) is fulfilled. Therefore up to two equilibria

$$x_i^{AH} = \left[\begin{array}{cccccccc} \bar{X}_S & 0 & \bar{X}_{A_i} & \bar{X}_{H_i} & S_{in} & 0 & 0 & 0 \end{array}\right]'$$

$$\xi_i^{AH} = \left[\begin{array}{cccccccc} \bar{X}_S & 0 & \bar{X}_{A_i} & \bar{X}_{H_i} & \bar{S} & \bar{V} & \bar{A}_i & \bar{H}_i \end{array}\right]'$$

may be obtained, where $\bar{X}_S$ and $\bar{S}$ are respectively computed with (A.2) and (A.1), $\bar{A}_i$ are given by (A.16), $\bar{V}$ is given by (A.21), while $\bar{X}_{A_i}$, $\bar{H}_i$ and

$\bar{X}_{H_i}$ are calculated as:

$$\bar{X}_{A_i} = 1/k_6 \cdot (k_4 \bar{X}_S - \bar{A}_i) \tag{A.29}$$
$$\bar{H}_i = D \cdot (K_H + \mu_A \bar{A}_i)/(m_H - D) \tag{A.30}$$
$$\bar{X}_{H_i} = 1/k_9 \cdot (k_7 \bar{X}_S - \bar{H}_i) \tag{A.31}$$

Provided that (A.6), (A.7), (A.14) and (A.24) hold, ξ_i^{AH} are physical steady states if additionally $\bar{X}_{A_i} \geq 0$ and $\bar{X}_{H_i} \geq 0$. These conditions are respectively equivalent to

$$k_1/k_4 \cdot \bar{A}_i + \bar{S} \leq S_{in} \tag{A.32}$$
$$k_1/k_7 \cdot \bar{H}_i + \bar{S} \leq S_{in} \tag{A.33}$$

8. $g_S(S) = D$, $X_V = 0$, $g_A(A) = D$, $X_H = 0$: This type of steady state is characterized by the wash-out of acetic bacteria and hydrogenotrophic methanogens. Methane is produced only through acetoclastic methanogenesis. In this case also at most two equilibrium points may be obtained if (A.14) holds. These equilibria have the form

$$x_i^A = \begin{bmatrix} \bar{X}_S & 0 & \bar{X}_{A_i} & 0 & S_{in} & 0 & 0 & 0 \end{bmatrix}'$$

$$\xi_i^A = \begin{bmatrix} \bar{X}_S & 0 & \bar{X}_{A_i} & 0 & \bar{S} & \bar{V} & \bar{A}_i & \bar{H} \end{bmatrix}'$$

with $\bar{X}_S$ and $\bar{S}$ given respectively by (A.2) and (A.1), $\bar{A}_i$ given by (A.16), $\bar{V}$ given by (A.21), $\bar{X}_{A_i}$ given by (A.29) and

$$\bar{H} = k_7 \bar{X}_S \tag{A.34}$$

ξ_i^A are physical steady states if (A.6), (A.7) and (A.14) and (A.32) are fulfilled.

9. $g_S(S) = D$, $g_V(V, H) = D$, $g_A(A) = D$, $g_H(H, A) = D$: This type of steady state is characterized by the presence of all microorganisms and the occurrence of all conversions described by the model. In practice, the operation of the anaerobic digestion system at such a steady state is desirable. This alternative leads to two equilibria

$$x_i^{VAH} = \begin{bmatrix} \bar{X}_S & \bar{X}_{V_i} & \bar{X}_{A_i} & \bar{X}_{H_i} & S_{in} & 0 & 0 & 0 \end{bmatrix}'$$

$$\xi_i^{VAH} = \begin{bmatrix} \bar{X}_S & \bar{X}_{V_i} & \bar{X}_{A_i} & \bar{X}_{H_i} & \bar{S} & \bar{V}_i & \bar{A}_i & \bar{H}_i \end{bmatrix}'$$

with $\bar{X}_S$ and $\bar{S}$ given respectively by (A.2) and (A.1), $\bar{A}_i$ given by (A.16), $\bar{H}_i$ given by (A.30) and

$$\bar{V}_i = D \cdot (K_V + \mu_H \bar{H}_i)/(m_V - D) \tag{A.35}$$

$$\bar{X}_{V_i} = 1/k_3 \cdot (k_2 \bar{X}_S - \bar{V}_i) \tag{A.36}$$

$$\bar{X}_{A_i} = 1/k_6 \cdot (k_4 \bar{X}_S + k_5 \bar{X}_{V_i} - \bar{A}_i) \tag{A.37}$$

$$\bar{X}_{H_i} = 1/k_9 \cdot (k_7 \bar{X}_S + k_8 \bar{X}_{V_i} - \bar{H}_i) \tag{A.38}$$

These are physical steady states if (A.6), (A.7), (A.12), (A.14), (A.24) hold and additionally $\bar{X}_{V_i} \geq 0$, $\bar{X}_{A_i} \geq 0$, $\bar{X}_{H_i} \geq 0$, which can be equivalently rewritten as

$$k_1/k_2 \bar{V}_i + \bar{S} \leq S_{in} \tag{A.39}$$

$$k_3 c_1 \bar{A}_i + k_5 c_1 \bar{V}_i + \bar{S} \leq S_{in} \tag{A.40}$$

$$k_3 c_2 \bar{H}_i + k_8 c_2 \bar{V}_i + \bar{S} \leq S_{in} \tag{A.41}$$

with c_1, c_2 defined above.

Appendix B. Calculation of the bifurcation diagram

ξ^0 is a physical equilibrium point if both (A.6) and (A.7) hold. In the plane (S_{in}, D) the boundary of (A.6) is represented by a horizontal line $D = m_S$ for all values of S_{in}, while the boundary of (A.7) is obtained by replacing (A.1) in (A.7): $DK_S/(m_S - D) = S_{in}$. These boundaries as well as the region where ξ^0 is physical are shown in Figure B.7.

ξ^V is a physical equilibrium point if (A.6), (A.7), (A.12) and (A.13) hold. As before, the boundary of (A.12) is represented by a horizontal line $D = m_V$ for all values of S_{in}, while the boundary of (A.13) needs some more developments. By replacing (A.8), (A.9), (A.11) and (A.2) in (A.13) one gets

$$\frac{k_1/k_2 DK_V/(m_V - D)}{1 - k_7/k_2 \mu_H D/(m_V - D)} = S_{in} - \bar{S} \tag{B.1}$$

Since the right hand term is positive as (A.7) holds and the nominator of the left hand term is positive as (A.12) holds, the denominator of (B.1) must be positive. This implies that (A.13) is fulfilled only if

$$D < D^V = k_2 m_V/(k_2 + \mu_H k_7) \tag{B.2}$$

The boundaries and the region where ξ^V is a physical equilibrium point are shown in Figure B.8.

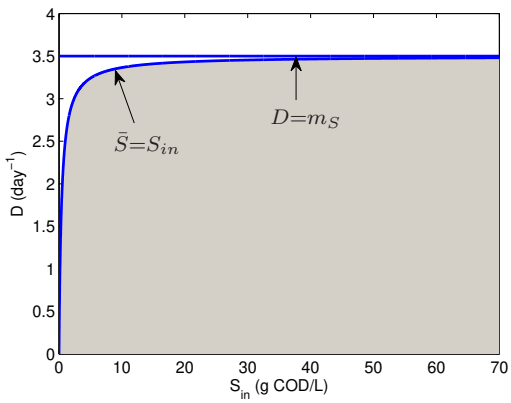

Figure B.7: The region in the input space for physical ξ^0

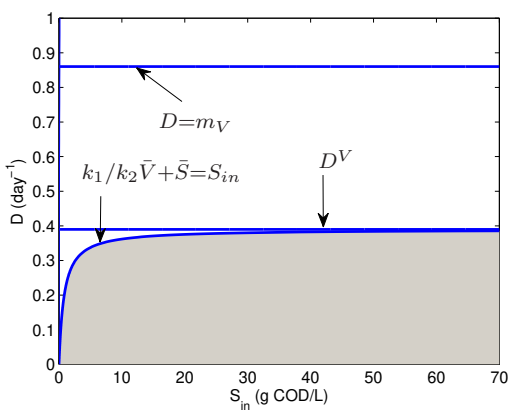

Figure B.8: The region in the input space for physical ξ^V

ξ_i^{VA} are physical equilibria if (A.6), (A.7), (A.12), (A.13), (A.14) and (A.19) are fulfilled. Note that ξ_i^{VA} and ξ^V are characterized by the same concentration of volatile fatty acids $\bar{V}$, which implies that condition (A.13) holds only if the dilution rate satisfies (B.2). Further on, (A.19) is developed in the same manner, by replacing $\bar{V}$ with its expression given by (A.8):

$$\frac{k_3 c_1 \bar{A}_i + k_5 c_1 D K_V/(m_V - D)}{1 - k_5 c_1 D/(m_V - D)\mu_H (k_3 k_7 + k_8 k_2)/(k_3 k_1)} = S_{in} - \bar{S} \tag{B.3}$$

and the same reasoning is applied, which leads to

$$D < D^{VA} = m_V/(1 - \mu_H(k_8/k_3 - k_5 c_1/(k_3 c_2))) \tag{B.4}$$

Taking into account all the conditions that the dilution rate must satisfy so far, one may summarize them as

$$D < \min\left(m_S, m_V, \max(g_A(A)), D^V, D^{VA}\right) \tag{B.5}$$

which is equivalent to $D < \max(g_A(A)) = g_A\left(\sqrt{K_A K_I}\right)$ for the parameter values considered in this study. Note that in the plane (S_{in}, D), (A.13) is monotonically increasing as shown also in Figure B.8, while (A.19) is monotonically increasing for $\bar{A} \leq \sqrt{K_A K_I}$ and monotonically decreasing for $\bar{A} > \sqrt{K_A K_I}$ due to the structure of $g_A(A)$. For $D = \max(g_A(A))$ both curves will reach their maximum value (due to the limitation (B.5) in case of (A.13) and its definition in case of (A.19)). The maximum value occurs at a lower substrate inlet concentration ($S_{in,1}^{VA}$) for (A.19) than for (A.13) ($S_{in,2}^{VA}$) as illustrated in Figure B.9. Hence, the two boundaries intersect at some point $S_{in}^{VA*} \in \left(S_{in,1}^{VA}, S_{in,2}^{VA}\right)$. To compute the intersection point, one sets (A.13) equal to (A.19), which leads to

$$\bar{A}_i^{VA*} = a_1 \bar{V}^{VA*} \tag{B.6}$$

where $\bar{A}_i^{VA*}$ and $\bar{V}^{VA*}$ represent the values of the states at the intersection point. Since the intersection point is a system equilibrium point, $\bar{A}_i^{VA*}$ and $\bar{V}^{VA*}$ must respectively satisfy (A.15) and (A.8). Thus,

$$\bar{V}^{VA*} = D^{VA*} K_V / \left(m_V - a_2 D^{VA*}\right) \tag{B.7}$$

In (B.6), (B.7), the coefficients a_1 and a_2 are defined as

$$\begin{aligned} a_1 &= (k_1 - k_2 k_5 c_1)/k_2 k_3 c_1 \\ a_2 &= 1 - \mu_H\left(k_8/k_3 - k_1/k_2 k_3 c_2\right) \end{aligned} \tag{B.8}$$

Using (B.6) and (B.7) in (A.15) leads to

$$a\left(D^{VA*}\right)^2 + bD^{VA*} + c = 0 \tag{B.9}$$

where

$$\begin{aligned} a &= a_1^2 K_V^2 - a_1 a_2 K_I K_V + K_A K_I a_2^2 \\ b &= a_1 K_I K_V m_V + a_1 a_2 K_I K_V m_A - 2a_2 K_A K_I m_V \\ c &= -a_1 K_I K_V m_A m_V + K_A K_I m_V^2 \end{aligned} \tag{B.10}$$

The solution of (B.9), which fulfills $D^{VA*} < \max(g_A)$ is the value of the dilution rate at the intersection point. The regions where ξ_i^{VA} are physical steady states are illustrated in Figure B.9. ξ_1^{VA} occurs as physical equilibrium point in the region lying below the increasing branch of (A.19) and below (A.13) (dark and light areas on Figure B.9). ξ_2^{VA} occurs as physical equilibrium point in the region lying above the decreasing branch of (A.19) and below (A.13) (light area on Figure B.9).

ξ^H is a physical equilibrium point when (A.6), (A.7), (A.24) and (A.25) hold simultaneously. To find out the range of dilution rates for which (A.25) is fulfilled, one uses (A.20) in (A.25) which leads to

$$\frac{k_1/k_7 D K_H/(m_H - D)}{1 - k_4/k_7 D \mu_A/(m_H - D)} = S_{in} - \bar{S} \tag{B.11}$$

When (B.11) holds, its denominator is positive, which implies that

$$D < D^H = m_H/(1 + k_4/k_7 \mu_A) \tag{B.12}$$

The region where ξ^H is a physical steady state is shown in Figure B.10.

ξ^{VH} is a physical steady state when (A.6), (A.7), (A.12), (A.13), (A.24) and (A.28) are fulfilled. Some of these conditions have been already discussed or are straightforward. The ones which need special attention are (A.13) and (A.28). Although (A.13) has been developed for previous equilibria, in this case the end condition on the dilution rate will be different due to the different expressions of the states at equilibrium. Thus, replacing the corresponding expressions of $\bar{V}$, $\bar{H}$ and $\bar{A}$ in (A.13) one gets

$$\frac{\frac{k_1/k_2 D(K_V(m_H - D) + \mu_H D K_H)}{((m_V - D)(m_H - D) + \mu_H \mu_A D^2 k_5/k_3)}}{1 - \frac{k_1/k_2 D^2 \mu_H \mu_A/(c_1 k_3)}{((m_V - D)(m_H - D) + \mu_H \mu_A D^2 k_5/k_3)}} = S_{in} - \bar{S} \tag{B.13}$$

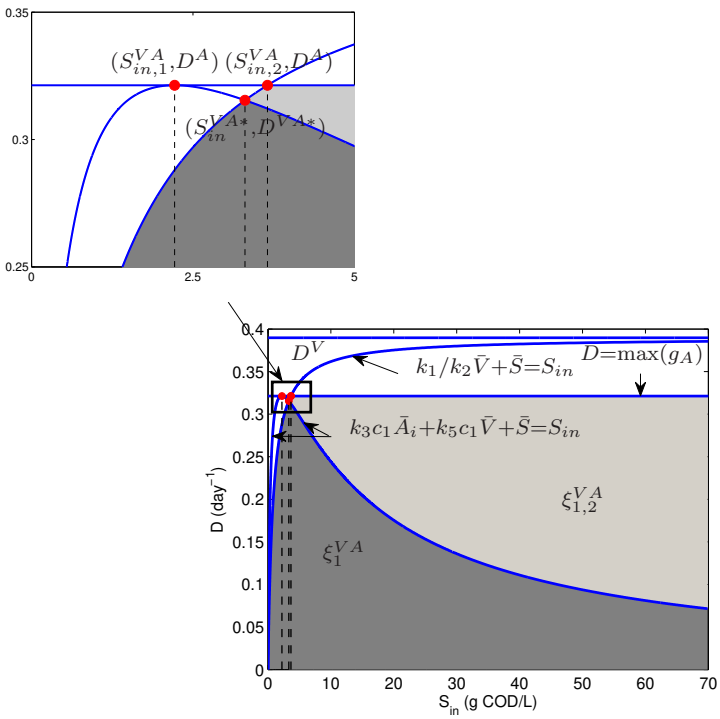

Figure B.9: The region in the input space for physical ξ_i^{VA}: darker region - only ξ_1^{VA} occurs, lighter region - both $\xi_{1,2}^{VA}$ occur

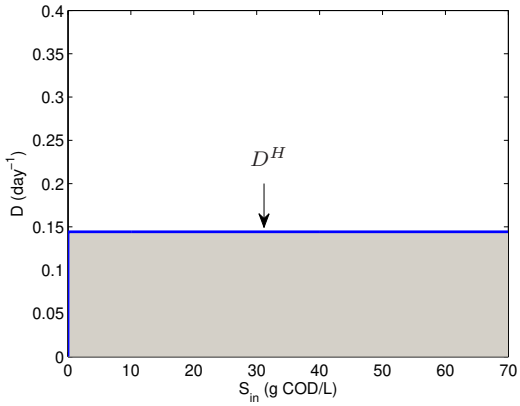

Figure B.10: The region in the input space for physical ξ^H

which is true only if the denominator is positive. This is rewritten as a quadratic inequality in D

$$aD^2 + bD + c < 0 \tag{B.14}$$

with

$$\begin{aligned} a &= (\mu_H \mu_A k_4/k_2 - 1) \\ b &= (m_V + m_H) \\ c &= -m_V m_H \end{aligned} \tag{B.15}$$

The change of sign in inequality (B.14) is performed such that the coefficient a becomes positive for the numerical values of the parameters given in Table 2. Inequality (B.14) holds for all values of D in the interval (D_1, D_2), where $D_{1,2}$ are the solutions of the equation associated to (B.14). Note that the sum and the product of the solutions, respectively given by $-b/a = -(m_V + m_H)/(\mu_H \mu_A k_4/k_2 - 1)$ and $c/a = -m_V m_H/(\mu_H \mu_A k_4/k_2 - 1)$, are negative, which implies that D_1 is negative and D_2 is positive. Since the dilution rate may assume only positive values, it is concluded that (A.13) holds for $0 \leq D < D_2 = D^{VH,1}$. $D^{VH,1}$ is given by

$$D^{VH,1} = \frac{-b + \sqrt{b^2 - 4ac}}{2a} \tag{B.16}$$

where the parameters are defined by (B.15). In a similar fashion, replacing the expressions of $\bar{H}$ and $\bar{V}$ corresponding to ξ^{VH} in (A.28) leads to:

$$\frac{k_3 c_2 \frac{DK_H}{(m_H - D)} + c_2 \left(k_8 - k_5 \frac{D\mu_A}{(m_H - D)}\right) \frac{D(K_V(m_H - D) + D\mu_H K_H)}{(m_H - D)(m_V - D)} + k_5/k_3 \mu_A \mu_H D^2}{1 - \frac{c_2 D\mu_A}{c_1(m_H - D)} - \frac{c_2}{k_3 c_1}\left(k_8 - k_5 \frac{D\mu_A}{(m_H - D)}\right) \frac{\mu_A \mu_H D^2}{(m_H - D)(m_V - D)} + k_5/k_3 \mu_A \mu_H D^2} = S_{in} - \bar{S} \tag{B.17}$$

which holds only if the denominator is positive. This condition can be rewritten again as a quadratic inequality in D of the form

$$aD^2 + bD + c > 0 \tag{B.18}$$

with

$$\begin{aligned} a &= (1 + (k_5/k_3 - (k_8 c_2)/(k_3 c_1))\, \mu_A \mu_H + (c_2/c_1)\mu_A) \\ b &= -\left(m_H + m_V + (c_2/c_1) m_V \mu_A\right) \\ c &= m_H m_V \end{aligned} \tag{B.19}$$

As the coefficient of D^2 in (B.18) is positive (for the numerical values used in this study), the sum and the product of the solutions D_1, D_2 of the equation associated to (B.18) are also positive. One may conclude that (B.18) holds for any $D \in [0, D_1) \cup (D_2, +\infty)$. Since the previous condition for the occurrence of ξ^{VH} imposed that the dilution rate must be smaller than $D^{VH,1}$, one could check whether $D^{VH,1}$ fulfills condition (B.18). If this is the case, then either $D^{VH,1} < D_1$ or $D^{VH,1} > D_2$. In the first situation $D^{VH,1}$ will be the highest dilution rate for which ξ^{VH} occurs, in the second case D_1 will be the highest dilution rate for which ξ^{VH} occurs. However, in our case $D^{VH,1}$ does not fulfill condition (B.18), which means that $D^{VH,1} \in (D_1, D_2)$. This implies that the highest dilution rate which allows the occurrence of ξ^{VH} is $D^{VH,2} = D_1$, given by

$$D^{VH,2} = \frac{-b - \sqrt{b^2 - 4ac}}{2a} \tag{B.20}$$

where the parameters are defined by (B.19).

If an intersection between the boundaries (A.13) and (A.28) exists, it may be determined by setting equal the two expressions, which leads to

$$k_3 c_2 \bar{H}^{VH*} + k_8 c_2 \bar{V}^{VH*} = (k_1/k_2)\bar{V}^{VH*} \tag{B.21}$$

where $\bar{V}^{VH*}$, $\bar{H}^{VH*}$ denote the values of the respective states at the intersection point. By replacing $\bar{H}^{VH*}$ with the expression of $\bar{H}$ corresponding to the equilibrium point ξ^{VH}, one may determine the relationship between $\bar{V}^{VH*}$ and the dilution rate D^{VH*} as

$$\bar{V}^{VH*} = \frac{k_3 c_2 K_H D^{VH*}}{((k_1/k_2) - k_8 c_2)(m_H - D^{VH*}) - (k_3 k_4/k_2) c_2 \mu_A D^{VH*}} \tag{B.22}$$

Since $\bar{V}^{VH*}$ is a value at equilibrium, $\bar{V}^{VH*} = \bar{V}$, which leads to the second order equation

$$a\left(D^{VH*}\right)^2 + bD^{VH*} + c = 0 \tag{B.23}$$

with

$$\begin{aligned} a &= K_V\left((k_1/k_2) - k_8 c_2 + (k_3 k_4/k_2) c_2 \mu_A\right) - \\ &\quad K_H\left(\mu_H\left((k_1/k_2) - k_8 c_2\right) + k_3 c_2\right) \\ b &= -K_V m_H\left(2\left((k_1/k_2) - k_8 c_2\right) + (k_3 k_4/k_2) c_2 \mu_A\right) + \\ &\quad K_H\left(\mu_H m_H\left((k_1/k_2) - k_8 c_2\right) + k_3 c_2\left(m_H + m_V\right)\right) \\ c &= K_V m_H^2\left((k_1/k_2) - k_8 c_2\right) - K_H k_3 c_2 m_H m_V \end{aligned} \tag{B.24}$$

The solution $D^{VH*} < \min\left(D^{VH,1}, D^{VH,2}\right)$ is the value of the dilution rate at the intersection point, as shown in Figure B.11. For dilution rates smaller than D^{VH*}, the active boundary is represented by (A.13), for dilution rates higher than D^{VH*} the active boundary is represented by (A.28).

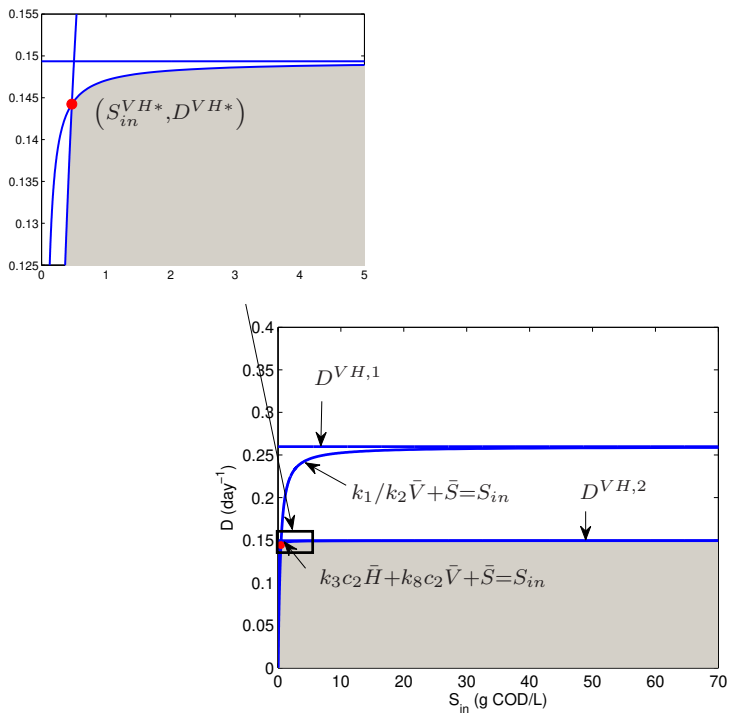

Figure B.11: The region in the input space for physical ξ^{VH}

ξ_i^A are physical steady states when (A.6), (A.7), (A.14) and (A.32) hold simultaneously. Note that the boundary of (A.32) may be rewritten as

$$\bar{A}_i = (k_4/k_1)\left(S_{in} - \bar{S}\right) \tag{B.25}$$

Since $\bar{A}_i$ is the state value at equilibrium, it must verify (A.15). Hence, by replacing $\bar{A}_i$ given by (B.25) in (A.15), one may calculate the values S_{in} corresponding to a certain dilution rate value $D < \max(g_A)$ by solving the second order equation

$$aS_{in}^2 + bS_{in} + c = 0 \tag{B.26}$$

with the coefficients given by

$$
\begin{aligned}
a &= (k_4/k_1)^2 \\
b &= -2DK_S/(m_S - D) \cdot (k_4/k_1)^2 + K_I(D - m_A)/D \cdot (k_4/k_1) \qquad \text{(B.27)} \\
c &= ((k_4/k_1) \cdot DK_S/(m_S - D))^2 - \\
&\qquad K_I(D - m_A)/D \cdot (k_4/k_1) \cdot DK_S/(m_S - D) + K_A K_I
\end{aligned}
$$

Thus, two branches are obtained which join together at the critical point $\left(S_{in}^{A*}, D^{A*}\right)$, where S_{in}^{A*} corresponding to $\bar{A} = \sqrt{K_A K_i}$ is given by

$$S_{in}^{A*} = \bar{S} + (k_1/k_4)\sqrt{K_A K_i} \qquad \text{(B.28)}$$

and $D^{A*} = \max(g_A)$. The regions where ξ_i^A are physical equilibria are shown in Figure B.12. ξ_1^A occurs as physical equilibrium point in the region below the increasing branch of the boundary (A.32) (dark and light areas on Figure B.12), ξ_2^A occurs as physical equilibrium point in the region above the decreasing branch of the boundary (A.32) (light area on Figure B.12).

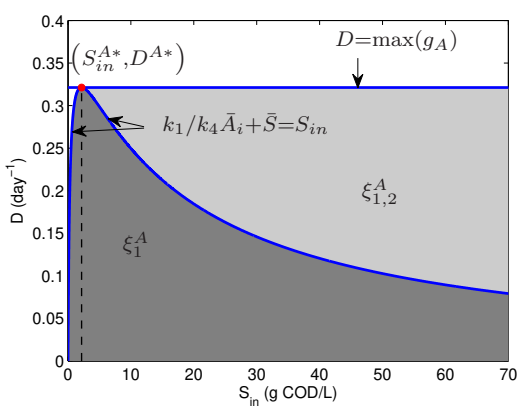

Figure B.12: The region in the input space for physical ξ_i^A: darker region - only ξ_1^A occurs, lighter region - both $\xi_{1,2}^A$ occur

ξ_i^{AH} are physical equilibria if (A.6), (A.7), (A.14), (A.24), (A.32) and (A.33) hold. Among the listed conditions only (A.32) and (A.33) are given in terms of values of states at equilibrium. Note that (A.32) is also a condition for the occurrence of ξ_i^A and it has been developed above. Thus, for dilution rates $D < \max(g_A)$ two S_{in} branches are obtained by solving (B.26) with

the parameters (B.27), which join together at the critical point $\left(S_{in}^{A*}, D^{A*}\right)$. Condition (A.33) may be developed in a similar way. Using the expression of $\bar{H}_i$ in the boundary of (A.33), $\bar{A}_i$ is calculated as

$$\bar{A}_i = \left((k_7/k_1) \cdot (m_H - D)/D \cdot (S_{in} - \bar{S}) - K_H\right)/\mu_A \tag{B.29}$$

By imposing that $\bar{A}_i$ given by (B.29) fulfils (A.15), a second order equation in S_{in} such as (B.26) is obtained. The parameters of this second order equation are

$$\begin{aligned} a &= ((k_7/k_1) \cdot (m_H - D)/D)^2 \\ b &= (k_7/k_1) \cdot (m_H - D)/D \left(-2\bar{S}(m_H - D)/D - 2K_H + \mu_A K_I (D - m_A)/D\right) \\ c &= (k_7/k_1) \cdot (m_H - D)/D \left((k_7/k_1) \cdot (m_H - D)/D \cdot \bar{S}^2 + 2K_H\bar{S} - \right. \\ &\quad \left. \mu_A K_I (D - m_A)/D\bar{S}\right) + K_H^2 - \mu_A K_I K_H (D - m_A)/D + \mu_A^2 K_A K_I \end{aligned} \tag{B.30}$$

Hence, the two branches of the boundary of (A.33) are given by the two solutions S_{in} obtained for dilution rates $D < \max(g_A)$, which join together at the critical point $\left(S_{in}^{AH}, D^{A*}\right)$. $D^{A*} = \max(g_A)$, while S_{in}^{AH} is the influent concentration which corresponds to $\bar{A} = \sqrt{K_A K_I}$ on the boundary (A.33):

$$S_{in}^{AH} = \bar{S} + (k_1/k_7) \cdot D^{A*}/(m_H - D^{A*}) \cdot \left(K_H + \mu_A\sqrt{K_A K_I}\right) \tag{B.31}$$

Intuitively, one may expect the occurrence of one or several intersections between the two boundaries, due to their characteristics. To compute the intersection points one sets equal the two boundaries, which implies

$$(k_1/k_7)\bar{H}_i^{AH*} = (k_1/k_4)\bar{A}_i^{AH*} \tag{B.32}$$

and determines the expression of acetic acid concentration as

$$\bar{A}_i^{AH*} = D^{AH*}K_H/\left((k_7/k_4)\left(m_H - D^{AH*}\right) - \mu_A D^{AH*}\right) \tag{B.33}$$

Next, using (B.33) in (A.15), a second order equation in D^{AH*} is obtained,

$$a\left(D^{AH*}\right)^2 + bD^{AH*} + c = 0 \tag{B.34}$$

with the parameters

$$
\begin{aligned}
a &= K_H^2 + \alpha \cdot \beta \\
b &= -(k_7/k_4) K_I m_H \beta - \alpha \cdot \gamma \\
c &= (k_7/k_4) K_I m_H \gamma \\
\alpha &= K_I \left((k_7/k_4) + \mu_A \right) \\
\beta &= K_A \left((k_7/k_4) + \mu_A \right) - K_H \\
\gamma &= (k_7/k_4) K_A m_H - K_H m_A
\end{aligned}
\tag{B.35}
$$

The solutions $D^{AH*} < \max(g_A)$ are the values of the dilution rate at the intersection points.

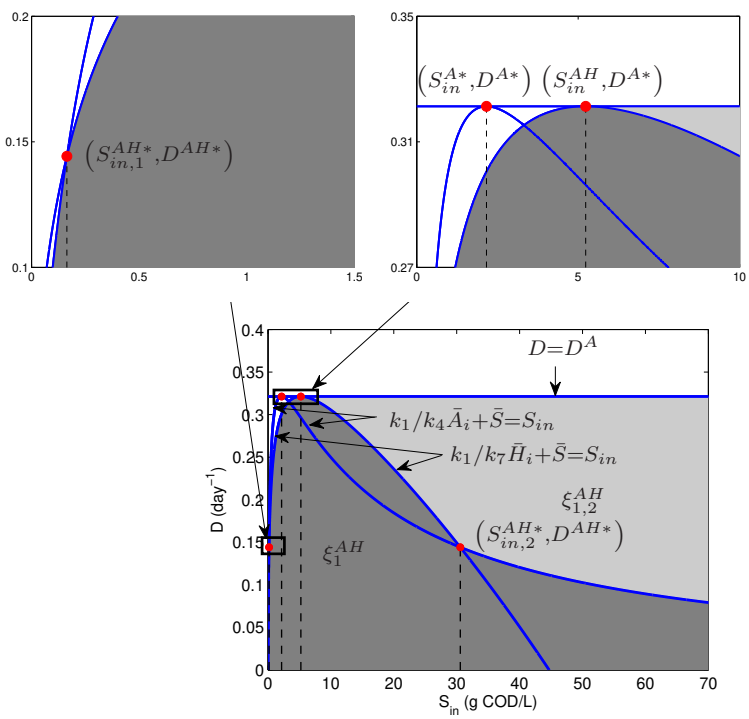

Figure B.13: The region in the input space for physical ξ_i^{AH}: darker region - only ξ_1^{AH} occurs, lighter region - both $\xi_{1,2}^{AH}$ occur

The boundaries and the regions where ξ_i^{AH} occur are illustrated in Figure B.13. ξ_1^{AH} occurs in the region below the increasing branches of the boundaries (A.32), (A.33) (dark and light areas on Figure B.13), while ξ_2^{AH}

occurs in the region above the decreasing branches of the boundaries (A.32), (A.33) (light area on Figure B.13). The intersections between the two boundaries occur at the dilution rate $D^{AH*} = 0.1442\text{day}^{-1}$. For dilution rates smaller than D^{AH*}, the active boundary is given by (A.32). For dilution rates higher than D^{AH*}, the active boundary is given by (A.33).

ξ_i^{VAH} are physical steady states if (A.6), (A.7), (A.12), (A.14), (A.24), (A.39), (A.40), (A.41) hold. Conditions (A.39)- (A.40) are expressed in terms of values of states at the equilibrium point. To obtain the expression of the boundaries which relates the dilution rate to the substrate inlet concentration the following procedure is applied: i) the expressions of the states at the equilibrium $\bar{V}_i$ and $\bar{H}_i$ are used in the boundary expressions and $\bar{A}_i$ is calculated as

$$\bar{A}_i = \frac{1}{\mu_a}\left(\frac{m_H - D}{D\mu_H}\left(\frac{k_1}{k_2}\frac{m_V - D}{D}\left(S_{in} - \bar{S}\right) - K_V\right) - K_H\right) \text{ for boundary (A.39)} \tag{B.36}$$

$$\bar{A}_i = \frac{1}{a_3}\left(S_{in} - a_4\right) \text{ for boundary (A.40)} \tag{B.37}$$

$$\bar{A}_i = \frac{1}{a_5}\left(S_{in} - a_6\right) \text{ for boundary (A.41)} \tag{B.38}$$

where a_3, a_4 are given by (B.39) and a_5, a_6 are given by (B.40);

$$a_3 = k_5 c_1 \mu_A \mu_H \frac{D^2}{(m_V - D)(m_H - D)} + k_3 c_1 \tag{B.39}$$
$$a_4 = \bar{S} + k_5 c_1 K_V \frac{D}{(m_V - D)} + k_5 c_1 \mu_H K_H \frac{D^2}{(m_V - D)(m_H - D)}$$

$$a_5 = k_3 c_2 \mu_A \frac{D}{(m_H - D)} + k_8 c_2 \mu_A \mu_H \frac{D^2}{(m_V - D)(m_H - D)} \tag{B.40}$$
$$a_6 = \bar{S} + k_3 c_2 \frac{D}{(m_H - D)} - k_8 c_2 K_V \frac{D}{(m_V - D)} - k_8 c_2 \mu_H K_H \frac{D^2}{(m_V - D)(m_H - D)}$$

ii) the derived expression for $\bar{A}_i$ must verify equation (A.15) which is used to compute the amount of acetic acid at equilibrium. Thus, for each boundary a second order equation in S_{in} is obtained, which has the form

$$\alpha\left(S_{in}\right)^2 + \beta S_{in} + \gamma = 0 \tag{B.41}$$

where the coefficients are respectively given by (B.42) for boundary (A.39), (B.43) for boundary (A.40) and (B.44) for boundary (A.41).

$$\alpha = a_1^2 \tag{B.42}$$
$$\beta = -2a_1^2\bar{S} - 2a_1a_2 + a_1\mu_A K_I \frac{(D-m_A)}{D}$$
$$\gamma = \left(a_1\bar{S} + a_2\right)^2 - a_1\mu_A K_I \bar{S}\frac{(D-m_A)}{D} - a_2\mu_A K_I \frac{(D-m_A)}{D} + \mu_A^2 K_A K_I$$
$$a_1 = \frac{k_1}{k_2}\frac{(m_H-D)(m_V-D)}{\mu_H D^2}$$
$$a_2 = K_V\frac{(m_H-D)}{\mu_H D} + K_H$$

$$\alpha = 1 \tag{B.43}$$
$$\beta = -2a_4 + K_I\frac{D-m_A}{D}a_3$$
$$\gamma = a_4^2 - K_I\frac{D-m_A}{D}a_3a_4 + a_3^2K_AK_I$$

$$\alpha = 1 \tag{B.44}$$
$$\beta = -2a_6 + K_I\frac{D-m_A}{D}a_5$$
$$\gamma = a_6^2 - K_I\frac{D-m_A}{D}a_5a_6 + a_5^2K_AK_I$$

iii) for each dilution rate $0 < D < D^{A*}$ two S_{in} branches are obtained, which join together at $\left(S_{in,1}^{VAH}, D^{A*}\right)$ on boundary (A.39), at $\left(S_{in,2}^{VAH}, D^{A*}\right)$ on boundary (A.40) and at $\left(S_{in,3}^{VAH}, D^{A*}\right)$ on boundary (A.41), with

$$V^{D^{A*}} = \frac{D^{A*}}{m_V - D^{A*}}\left(K_V + \mu_H\frac{D^{A*}}{m_H - D^{A*}}\left(K_H + \mu_A\sqrt{K_AK_I}\right)\right)$$
$$S_{in,1}^{VAH} = \frac{k_1}{k_2}V^{D^{A*}} + K_S\frac{D^{A*}}{m_S - D^{A*}} \tag{B.45}$$
$$S_{in,2}^{VAH} = k_5c_1V^{D^{A*}} + k_3c_1\sqrt{K_AK_I} + K_S\frac{D^{A*}}{m_S - D^{A*}}$$
$$S_{in,3}^{VAH} = k_8c_2V^{D^{A*}} + k_3c_2\frac{D^{A*}}{m_H - D^{A*}}\left(K_H + \mu_A\sqrt{K_AK_I}\right) + K_S\frac{D^{A*}}{m_S - D^{A*}}$$

To compute the intersections between two boundaries a similar algorithm is followed: firstly, the expressions of the two boundaries are set equal; secondly, the concentration of acetic acid at the intersection point $\bar{A}_i^{VAH*}$ is computed as an expression depending on the dilution rate D; thirdly, the expression of $\bar{A}_i^{VAH*}$ must verify (A.15) since $\bar{A}_i^{VAH*}$ is the value at an equilibrium point. Thus, a higher order equation in the dilution rate is obtained, which has the form

$$A_1 \left(D^{VAH*}\right)^4 + A_2 \left(D^{VAH*}\right)^3 + A_3 \left(D^{VAH*}\right)^2 + A_4 \left(D^{VAH*}\right) + A_5 = 0 \tag{B.46}$$

The solutions $0 < D^{VAH*} < D^{A*}$ represent the values of the dilution rate at the intersection points, which can be used to compute further the corresponding S_{in}^{VAH*}.

Hence, at the intersection point(s) between (A.39) and (A.40), the acetic acid concentration is given by

$$\bar{A}_i^{VAH*} = a_1 \frac{D^{VAH*} K_V (m_H - D^{VAH*}) + \mu_H K_K (D^{VAH*})^2}{k_3 c_1 (m_V - D^{VAH*})(m_H - D^{VAH*}) - a_1 \mu_A \mu_H (D^{VAH*})^2} \tag{B.47}$$

while the coefficients of (B.46) are defined as follows:

$$\begin{aligned}
A_1 &= a_1^2 \alpha^2 - a_1 K_I K_V \beta + K_A K_I \beta^2 \qquad \text{(B.48)}\\
A_2 &= -2a_1^2 K_V m_H \alpha + a_1 K_I (\beta\gamma + k_3 c_1 K_V \delta) - 2K_A K_I k_3 c_1 \beta\delta \\
A_3 &= a_1^2 K_V^2 m_H^2 - a_1 K_I (k_3 c_1 \delta\gamma + m_A \beta(\gamma - K_V m_A) + K_V \epsilon) + K_A K_I ((k_3 c_1 \delta)^2 + 2\epsilon\beta) \\
A_4 &= a_1 K_I (k_3 c_1 (\gamma - K_V m_A)(m_V m_H + m_A m_V + m_A m_H) + K_V m_A \epsilon) - 2K_A K_I k_3 c_1 \delta\epsilon \\
A_5 &= -a_1 K_I m_A \epsilon (\gamma - K_V m_A) + K_A K_I \epsilon^2
\end{aligned}$$

The following notations are used in (B.47), (B.48):

$$\begin{aligned}
a_1 &= \frac{k_1}{k_2} - k_5 c_1 & \alpha &= K_V - \mu_H K_H \qquad \text{(B.49)}\\
\beta &= k_3 c_1 - a_1 \mu_A \mu_H & \gamma &= K_V m_H + \mu_H K_H + K_V m_A \\
\delta &= m_V + m_H & \epsilon &= k_3 c_1 m_V m_H
\end{aligned}$$

At the intersection point(s) between (A.39) and (A.41), the expression of acetic acid concentration reads

$$\bar{A}_i^{VAH*} = \frac{a_2 K_V (m_H - D^{VAH*}) + a_2 \mu_H K_H D^{VAH*} - k_3 c_2 K_H (m_V - D^{VAH*})}{k_3 c_2 \mu_A (m_V - D^{VAH*}) - a_2 \mu_A \mu_H D^{VAH*}} \tag{B.50}$$

and the coefficients of (B.46) are given by:

$$
\begin{aligned}
A_1 &= 0 \\
A_2 &= \alpha^2 + K_I\alpha\gamma + K_AK_I\gamma^2 \\
A_3 &= 2\alpha\beta + K_I(-k_3c_2\mu_Am_V\alpha - k_3c_2\mu_Am_H(\alpha + a_2\mu_HK_H) + a_2\mu_A\mu_H\beta - \\
&\qquad m_A\alpha\gamma - 2K_Ak_3c_2\mu_Am_V\gamma) \\
A_4 &= \beta^2 + K_Ik_3c_2\mu_Am_Vm_H(\alpha + a_2\mu_HK_H) - K_Im_A(-k_3c_2\mu_Am_V\alpha - \\
&\qquad k_3c_2\mu_Am_H(\alpha + a_2\mu_HK_H) + a_2\mu_A\mu_H\beta) + K_AK_I(k_3c_2\mu_Am_V)^2 \\
A_5 &= -K_Im_Ak_3c_2\mu_Am_Vm_H(\alpha + a_2\mu_HK_H)
\end{aligned} \tag{B.51}
$$

The following notations are used in (B.50), (B.51):

$$
\begin{aligned}
a_2 &= \frac{k_1}{k_2} - k_8c_2 & \alpha &= a_2K_V - a_2\mu_HK_H - k_3c_2K_H \\
\beta &= k_3c_2K_Hm_V - a_2K_Vm_H & \gamma &= k_3c_2\mu_A + a_2\mu_A\mu_H
\end{aligned} \tag{B.52}
$$

At the intersection point(s) between (A.40) and (A.41) one has

$$
\bar{A}_i^{VAH*} = \frac{a_3K_VD^{VAH*}(m_H) - D^{VAH*} - k_3c_2K_HD^{VAH*}(m_V - D^{VAH*}) + a_3\mu_HK_H(D^{VAH*})^2}{k_3c_2\mu_AD^{VAH*}(m_V - D^{VAH*}) - k_3c_1(m_V - D^{VAH*})(m_H - D^{VAH*}) - a_3\mu_A\mu_H(D^{VAH*})^2} \tag{B.53}
$$

and the coefficients of (B.46) become:

$$
\begin{aligned}
A_1 &= \alpha^2 - K_I\alpha\gamma + K_AK_I\gamma^2 \\
A_2 &= 2\alpha\beta + K_I(\alpha\delta - \gamma\beta) + K_Im_A\alpha\gamma - 2K_AK_I\gamma\delta \\
A_3 &= \beta^2 + K_I(-\epsilon\alpha + \beta\delta) - K_Im_A(\alpha\delta - \gamma\beta) + K_AK_I(\delta^2 + 2\epsilon\gamma) \\
A_4 &= -K_I\epsilon\beta - K_Im_A(-\epsilon\alpha + \beta\delta) - 2K_AK_I\epsilon\delta \\
A_5 &= K_Im_A\epsilon\beta + K_AK_I\epsilon^2
\end{aligned} \tag{B.54}
$$

The notations employed in (B.53), (B.54) are defined as:

$$
\begin{aligned}
a_3 &= k_5c_1 - k_8c_2 & \alpha &= k_3c_2K_H + a_3\mu_HK_H - a_3K_V \\
\beta &= a_3K_Vm_H - k_3c_2K_Hm_V & \gamma &= k_3c_2\mu_A + k_3c_1 + a_3\mu_A\mu_H \\
\delta &= k_3c_1m_V + k_3c_1m_H + k_3c_2\mu_Am_V & \epsilon &= k_3c_1m_Vm_H
\end{aligned} \tag{B.55}
$$

Note that not all the intersection points between conditions (A.39)- (A.41) are bifurcation points, ie. lying on the active boundary and subsequently determining a switch to another boundary. ξ_1^{VAH} is a physical steady state in

the region lying below all the increasing branches of (A.39)- (A.41), while ξ_2^{VAH} is a physical steady state in the region lying above all decreasing branches of conditions (A.39)- (A.41), as illustrated in Figure B.14. One can determine the active boundary either considering a certain dilution rate or a certain substrate inlet concentration. For a certain dilution rate D, the active boundary will lead to the highest value of S_{in}. For a certain value of the substrate inlet concentration S_{in}, the active boundary will lead to the lowest value of the dilution rate D along the increasing branches and to the highest value of D along the decreasing branches. Hence, along the increasing branches condition (A.39) is the active boundary for dilution rates smaller than D_1^{VAH*}, while condition (A.41) is the active boundary for dilution rates higher than D_1^{VAH*}. Thus, $D_1^{VAH*} = 0.3150\text{day}^{-1}$ is calculated from the intersection of (A.39) with (A.41), ie. D_1^{VAH*} is a solution of (B.46) with the parameters given by (B.51), (B.52). Along the decreasing branches, condition (A.40) is the active boundary for dilution rates smaller than D_2^{VAH*}, while condition (A.41) is the active boundary for dilution rates higher than D_2^{VAH*}. Thus, $D_2^{VAH*} = 0.1493\text{day}^{-1}$ is a solution of (B.46) with the parameters (B.54), (B.55), which characterize the intersection between (A.40) and (A.41).

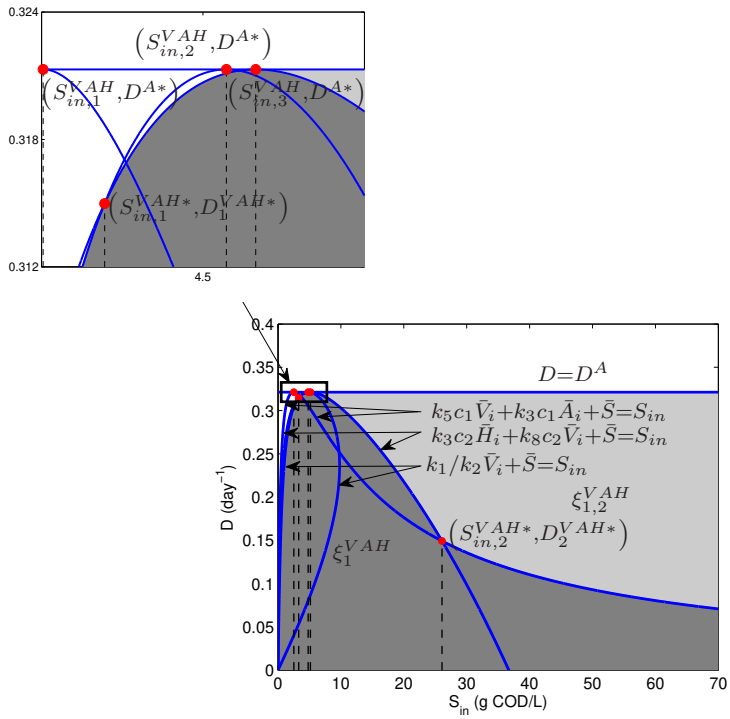

Figure B.14: The region in the input space for physical ξ_i^{VAH}: darker region - only ξ_1^{VAH} occurs, lighter region - both $\xi_{1,2}^{VAH}$ occur